Supporting Information
For the Manuscript

Selective recognition of Fe^{3+} and CrO_4^{2-} ions using Zn(II) metallacycle and Cd(II) coordination polymer and their heterogeneous catalytic application†

*Pooja Rani,[a||] Anjali Sharma,[a||] Ahmad Husain,[b] Gulshan Kumar,[a] Harpreet Kaur,[b] K. K. Bhasin[a] and Girijesh Kumar[*a]*

[a]*Department of Chemistry & Centre for Advanced Studies in Chemistry, Panjab University, Chandigarh–160014, India. E-mail: gkumar@pu.ac.in.*

[b]*Department of Chemistry, DAV University, Jalandhar, Punjab–144012, India.*

Contents:

Synthesis of N,N'-bis-(3-pyridyl)terephthalamide (L). The ligand **L** has been synthesized using the literature procedure with slight modification.[1,2] The terephthallic acid (0.2g, 1.2 mmol) and 3-aminopyridine (0.25g, 2.6 mmol) were mixed in 6 mL of pyridine and refluxed for 30–40 minutes. After that $P(OPh)_3$ was added as a coupling agent and refluxing was continued for 24 h (See Scheme 1). The progress of the reaction was monitored by thin layer chromatography (TLC). After completion of reaction, ice cold water was added to it giving white colour precipitates. The precipitates were filtered off, washed with diethyl ether and dried and further re-crystallized from methanol. Yield: 0.218g (57%; based on terephthallic acid). FT-IR (ν cm^{-1}): 1678, 1653 (C=O), 1559 (N–H). UV-Vis (DMSO), λ_{max}/nm: 280–290 nm. ^{1}H NMR (400 MHz, DMSO-d_6): δppm 7.42 – 7.45 (dd, 2H, H_b, J = 8.44 & 4.95 Hz), 8.15 (s, 4H, H_f), 8.23 (d, 2H, H_c, J = 8.86 Hz), 8.36 (d, 2H, H_a), 8.97 (m, 2H, H_d), 10.64 (s, 2H, H_e).

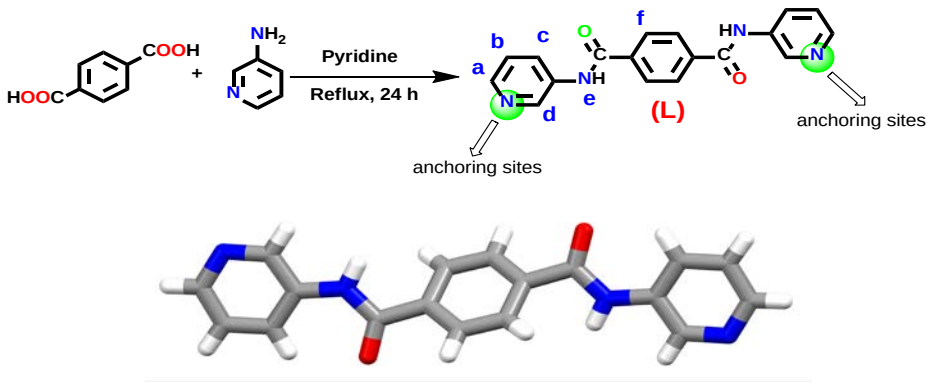

Scheme S1. Synthetic route of amide-based ligand **L**.

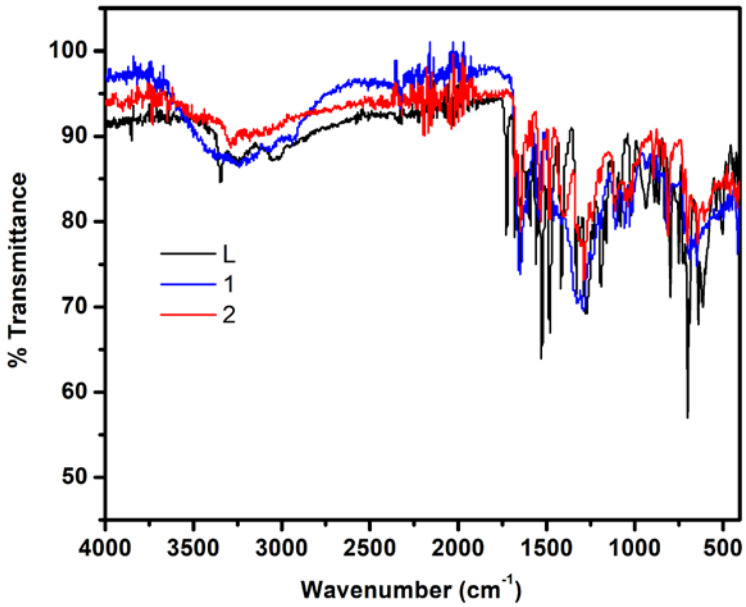

Fig. S1. FT-IR spectra of ligand **L** and coordination compounds **1** and **2**.

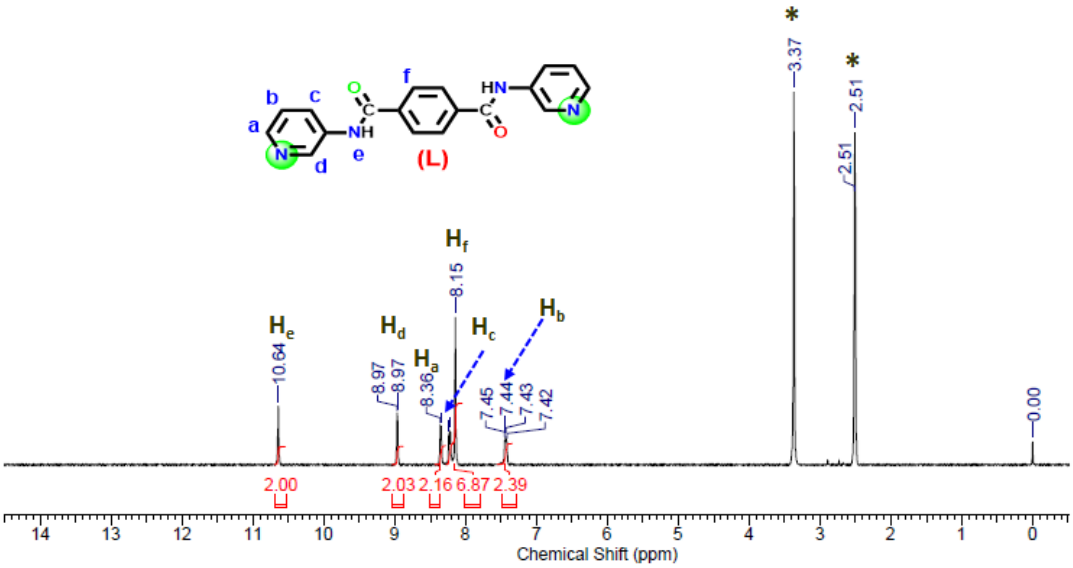

Fig. S2. ^{1}H NMR spectrum of ligand **L** in DMSO-d_6. *Represents the solvent residual peak.

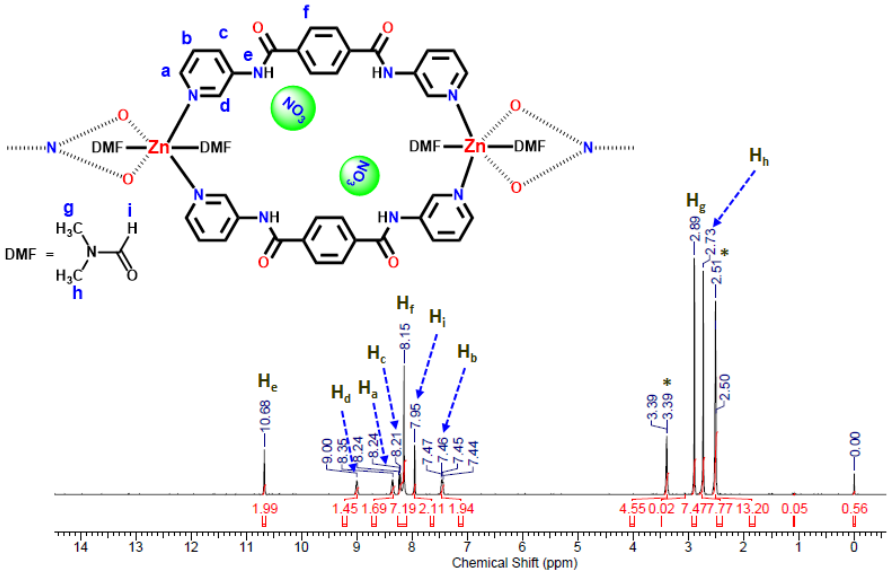

Fig. S3. ^{1}H NMR spectrum of **1** in DMSO-d_6. *Represents the solvent residual peak.

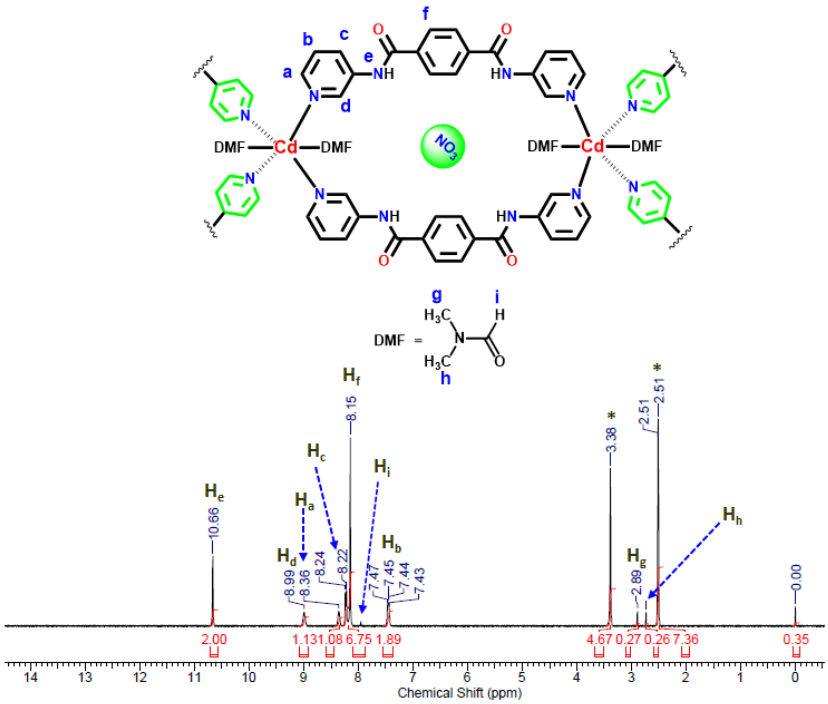

Fig. S4. ^{1}H NMR spectrum of **2** in DMSO-d_6. *Represents the solvent residual peak.

FLASH EA 1112 SERIES CHN REPORT
THERMO FINNIGAN

Method filename:	C:\Program Files\Thermo Finnigan\Eager 300 for EA1112\DATA\Sys_data_ex
Sample ID:	A1-ZN (# 7)
Analysis type:	UnkNown
Chromatogram filename:	UNK-30042019-7.dat
Sample weight:	1.183

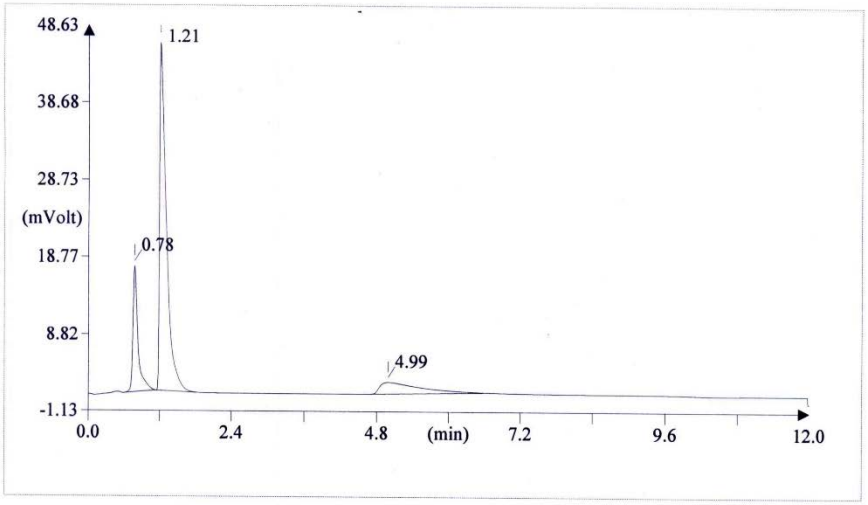

Element Name	Element %	Ret. Time
Nitrogen	17. 21	0. 78
Carbon	44. 15	1. 21
Hydrogen	4. 26	4. 99

Fig. S5. CHN plot for the metallacycle **1**.

FLASH EA 1112 SERIES CHN REPORT
THERMO FINNIGAN

Method filename:	C:\Program Files\Thermo Finnigan\Eager 300 for EA1112\DATA\Sys_data_ex
Sample ID:	A1-CD (# 6)
Analysis type:	UnkNown
Chromatogram filename:	UNK-30042019-6.dat
Sample weight:	1.172

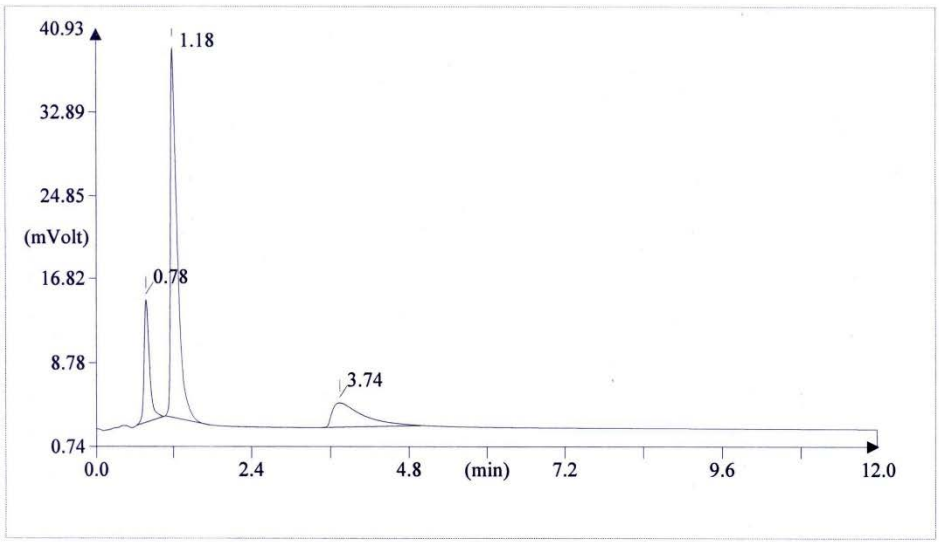

Element Name	Element %	Ret. Time
Nitrogen	16. 58	0. 78
Carbon	49. 62	1. 18
Hydrogen	4. 21	3. 74

Fig. S6. CHN plot for the coordination polymer **2**.

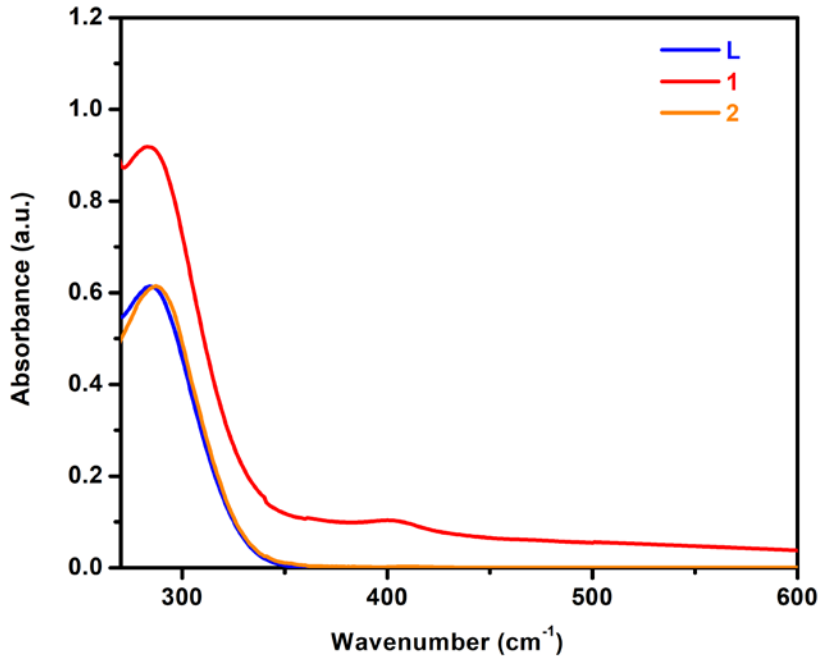

Fig. S7. UV-vis plots for compounds **1** and **2** along with **L**.

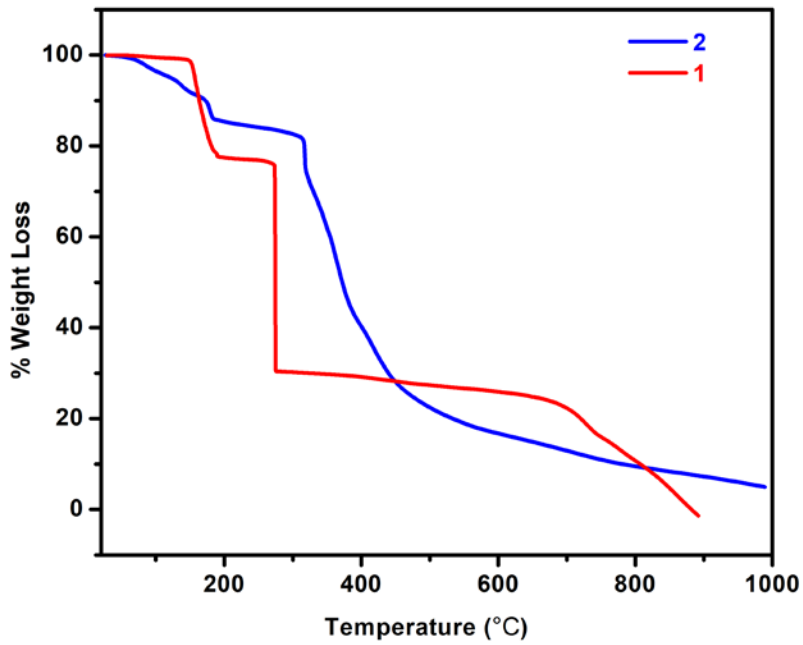

Fig. S8. TGA plots for compounds **1** and **2**.

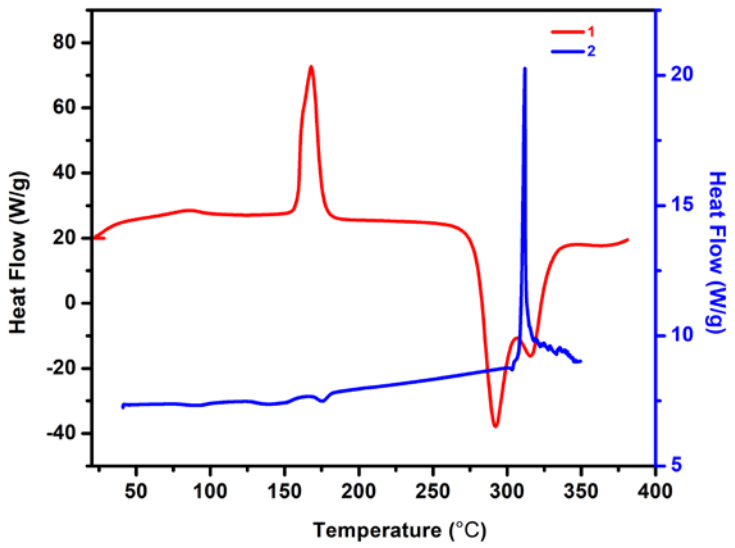

Fig. S9. DSC plot for compounds **1** and **2**.

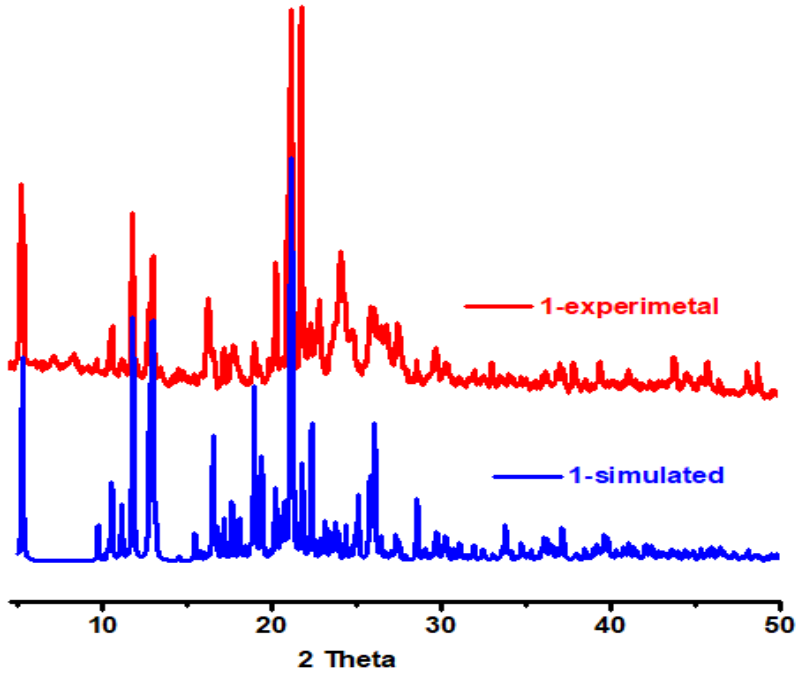

Fig. S10. PXRD pattern for metallacycle **1**, bulk sample (red trace) and the one simulated from the single crystal structure analysis (blue trace) using Mercury 4.0.

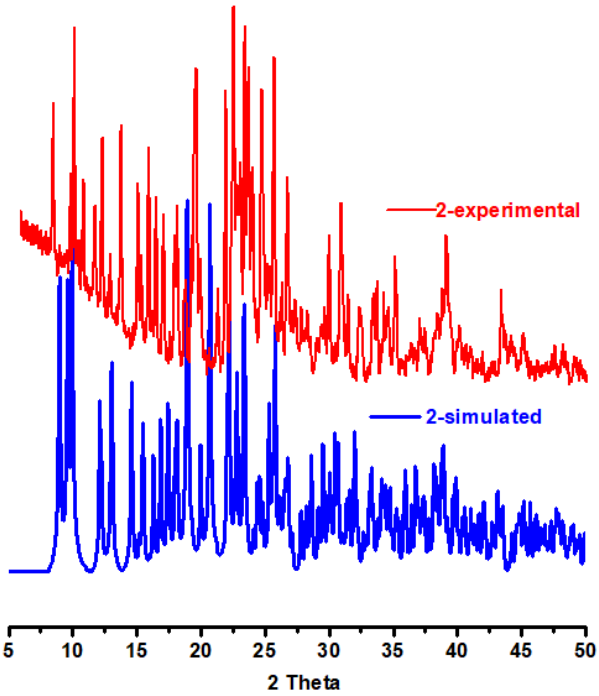

Fig. S11. PXRD pattern for coordination polymer **2**, bulk sample (red trace) and the one simulated from the single crystal structure analysis (blue trace) using Mercury 4.0.

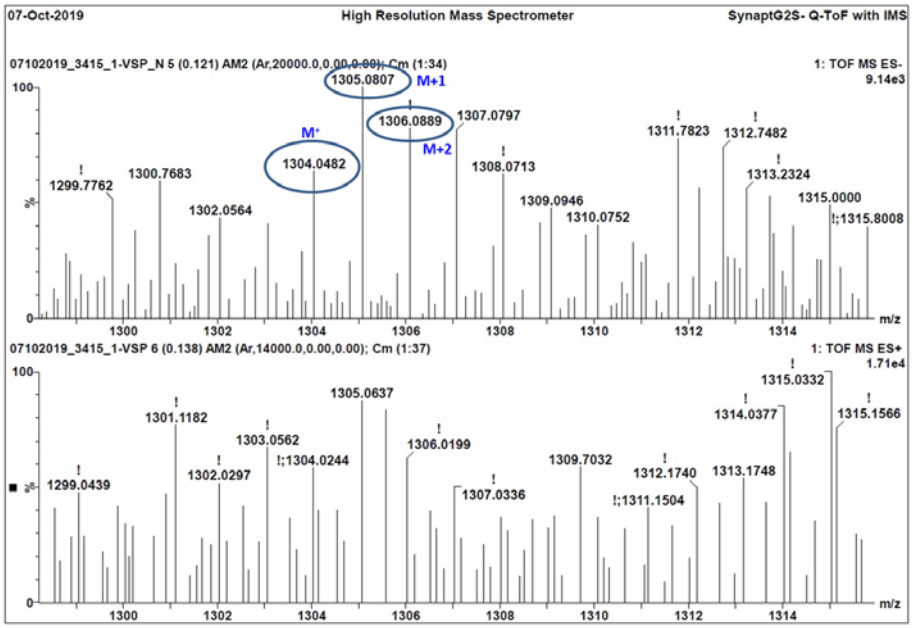

Fig. S12. HR mass spectrum of **1**. MS (ESI-TOF): calculated m/z for $[M]^+$ = 1304.2439, found = 1304.0482.

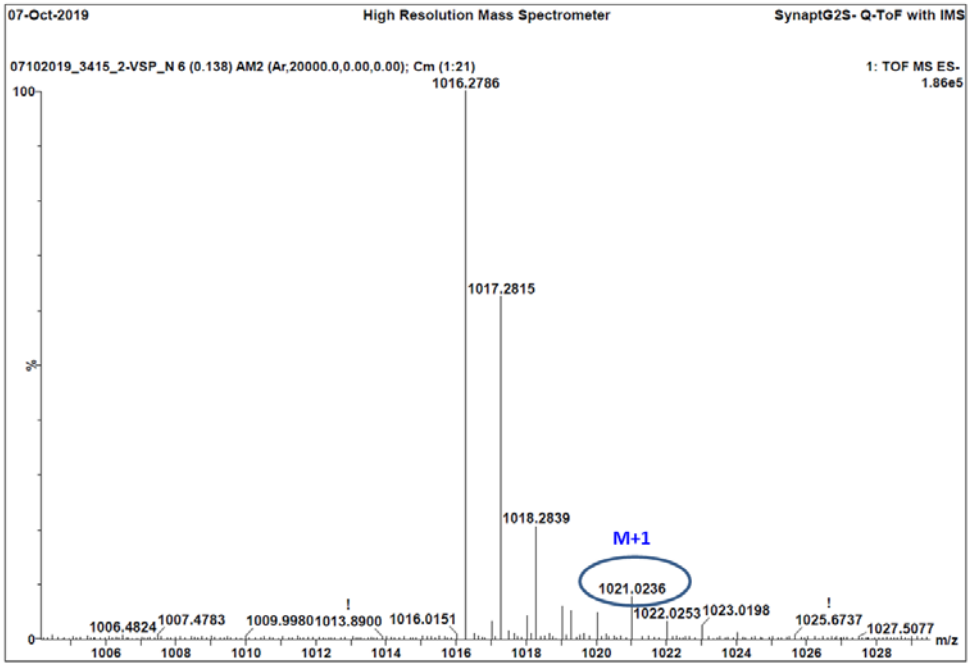

Fig. S13. HR mass spectrum of **2**. MS (ESI-TOF): calculated m/z for $[M+1]^+$ = 1021.2079, found = 1021.0236.

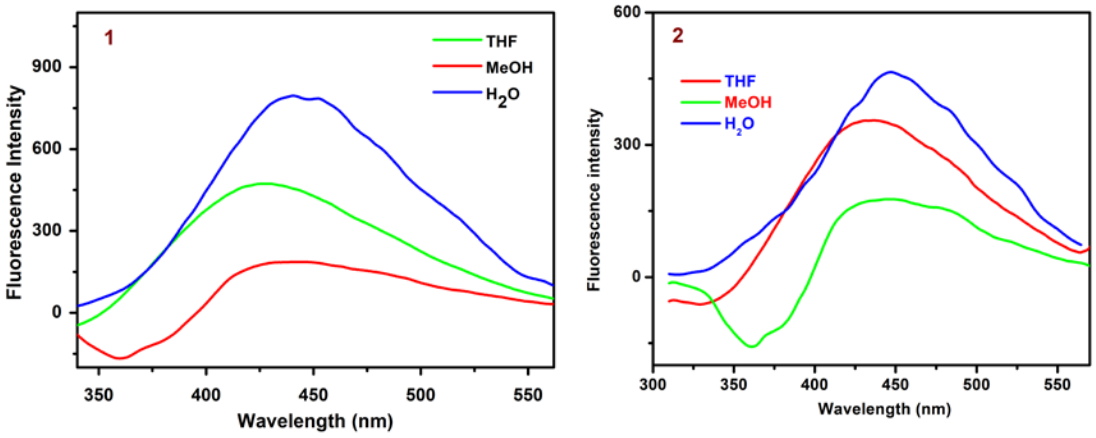

Fig. S14. Solvent scan to get the maximum fluorescence intensity for **1** (left) and **2** (right).

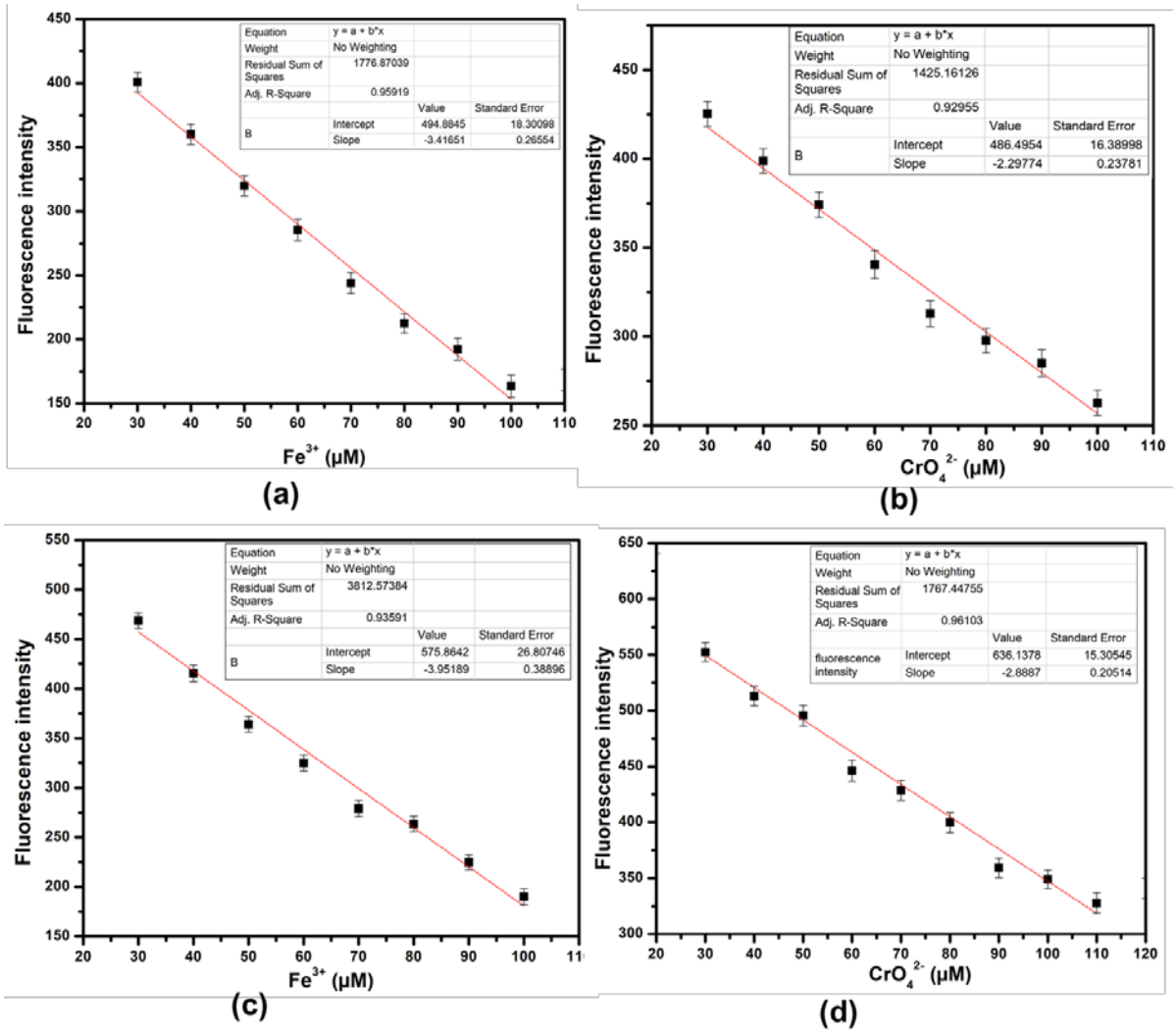

Fig. S15. Detection limit for the cation (Fe^{3+}) and anion (CrO_4^{2-}) with receptor **1** (a,b) and with **2** (c,d), respectively.

Determination of Stern–Volmer constant (K_{SV}) and detection limit.

Evolution of fluorescence titrations using the Stern– Volmer equation (1).[3]

$$\frac{I_0}{I} = 1 + K_{SV}[Q] \qquad (1)$$

Where, I_0 = emission intensity in the absence of quencher

I = emission intensity in the presence of quencher (Q)

K_{SV} = Stern–Volmer constant

The detection limit for the recognition of Fe^{3+} and IO_4^- ions were calculated by eqn (2).[4,5]

$$\text{Detection limit: } 3\sigma/k \qquad (2)$$

Where, σ = standard deviation of a blank measurements

k = slope of a plot of fluorescence intensity *versus* metal ion concentration.

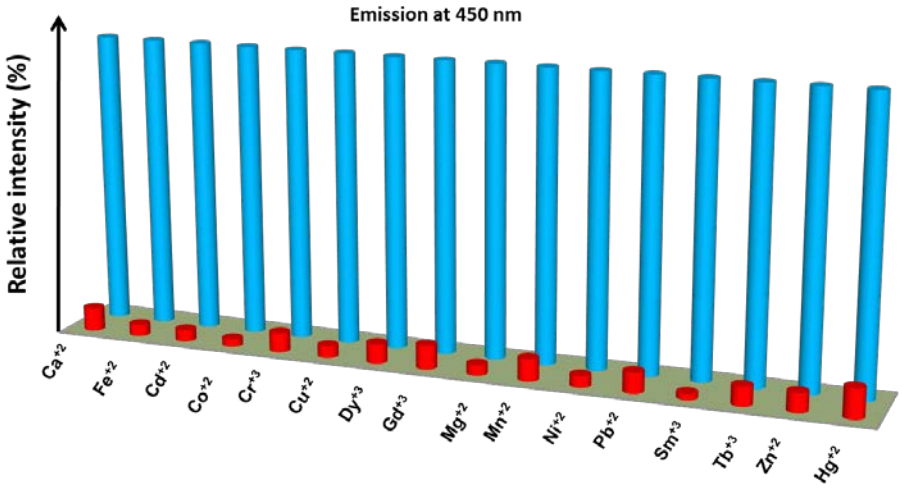

Fig. S16. Bar diagram representation of the relative fluorescence intensity of a suspension of **1** (2 mL) upon addition of 60 µL of 10 mM solution of $FeCl_3$ in the presence of 60 µL of 10 mM solution of background cations (M^{n+}) in aqueous media.

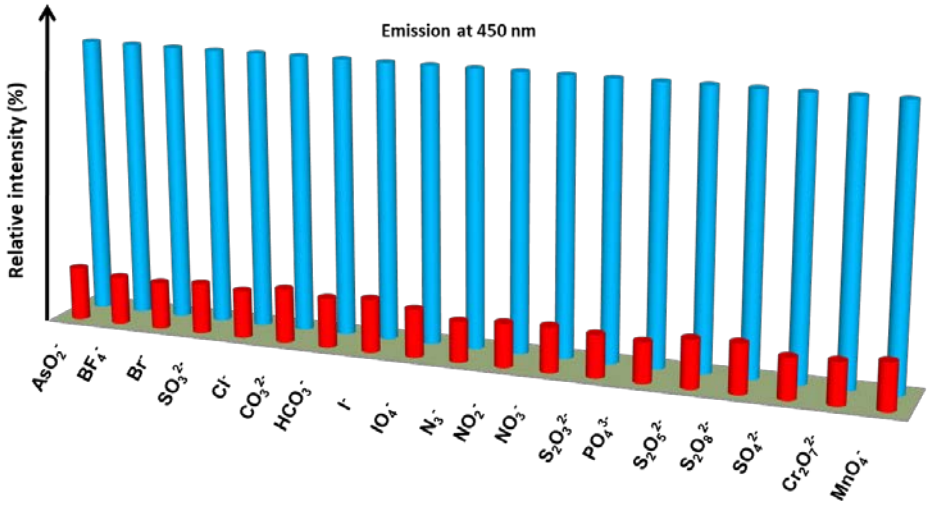

Fig. S17. Bar diagram representation of the relative fluorescence intensity of a suspension of **1** (2 mL) upon addition of 60 µL of 10 mM solution of K_2CrO_4 in the presence of 60 µL of 10 mM solution of background anions (A^{n-}) in aqueous media.

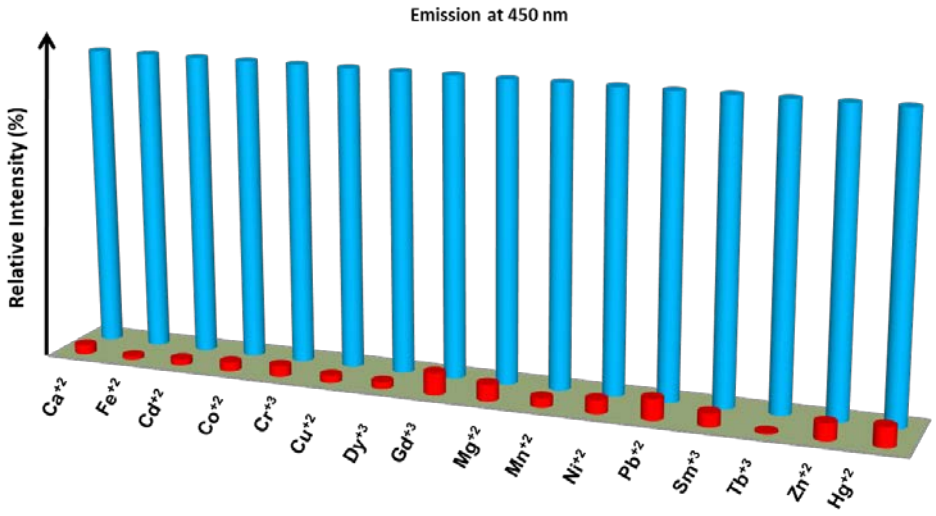

Fig. S18. Bar diagram representation of the relative fluorescence intensity of a suspension of **2** (2 mL) upon addition of 60 µL of 10 mM solution of $FeCl_3$ in the presence of 60 µL of 10 mM solution of background cations (M^{n+}) in aqueous media.

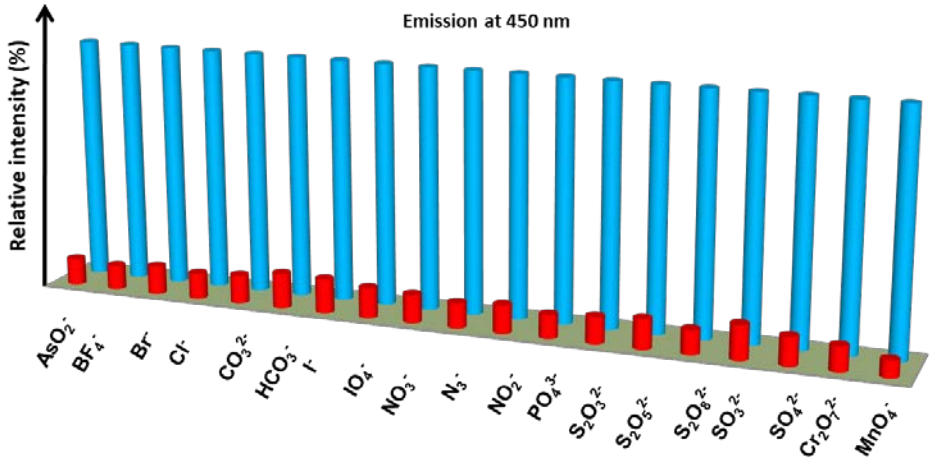

Fig. S19. Bar diagram representation of the relative fluorescence intensity of a suspension of **2** (2 mL) upon addition of 60 µL of 10 mM solution of K_2CrO_4 in the presence of 60 µL of 10 mM solution of background anions (A^{n-}) in aqueous media.

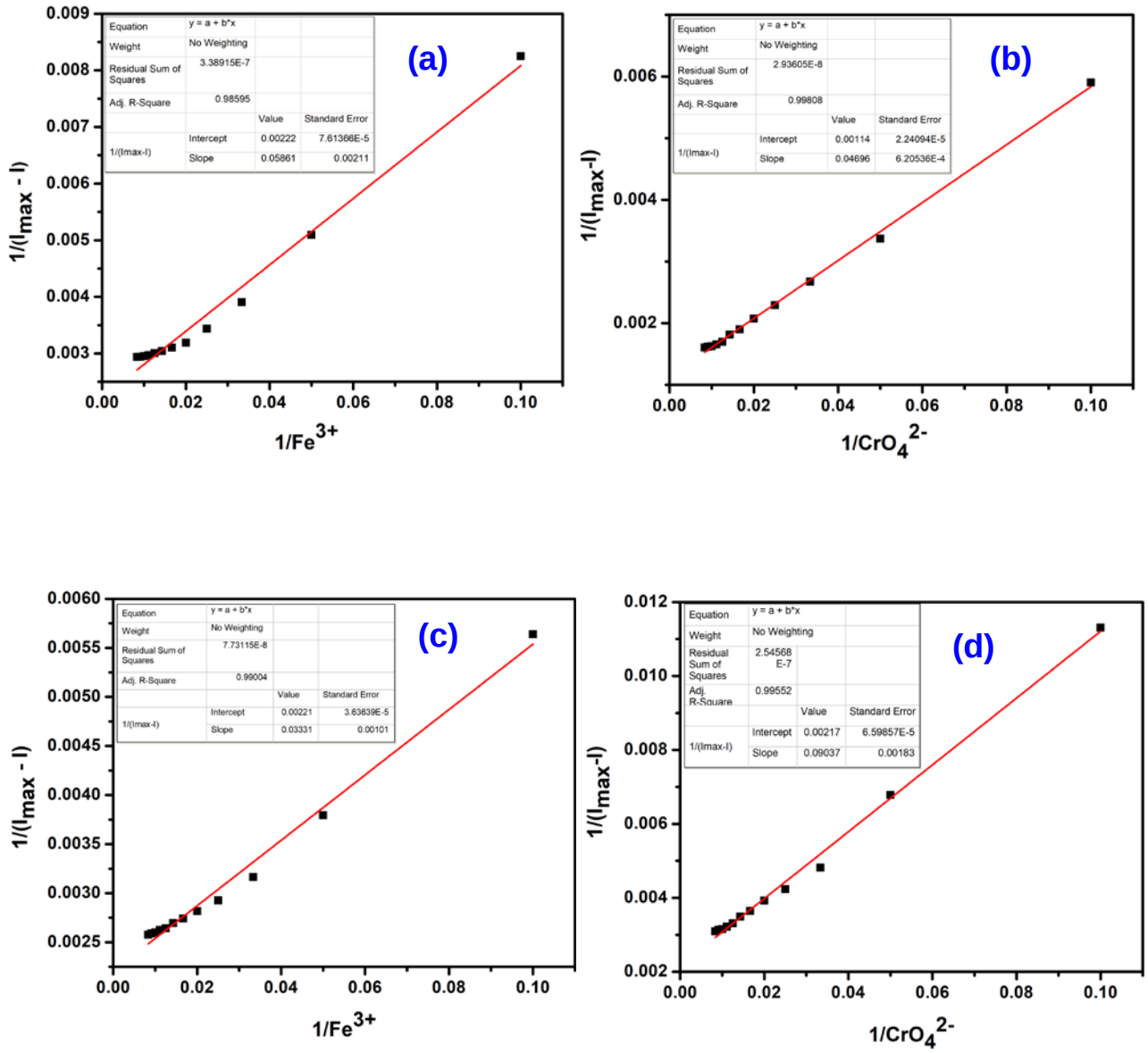

Fig. S20. Benesi–Hildebrand plots for the analysis of binding constant (K_b) for the detection of Fe^{3+} and CrO_4^{2-} ion with receptors **1** (a,b) and **2** (c,d), respectively.

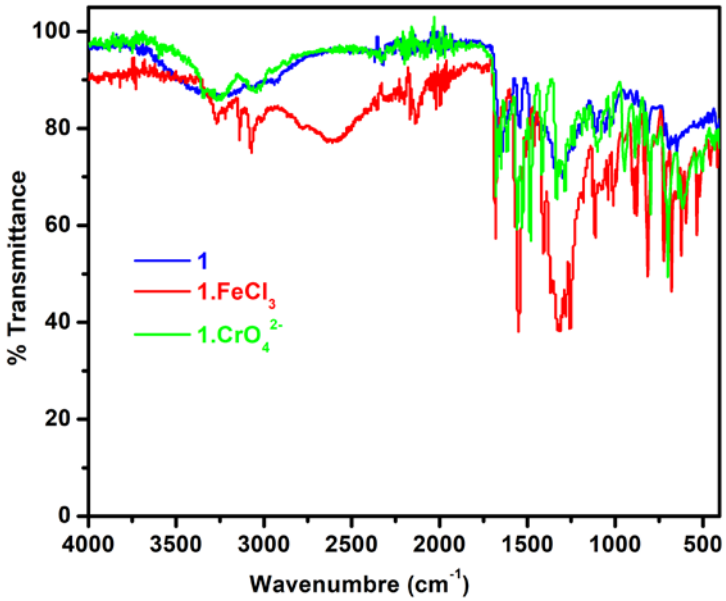

Fig. S21. FT-IR spectra of original sample of **1** (blue trace) and the recovered samples of **1** from the $FeCl_3$ (red trace) and CrO_4^{2-} (green trace) solution.

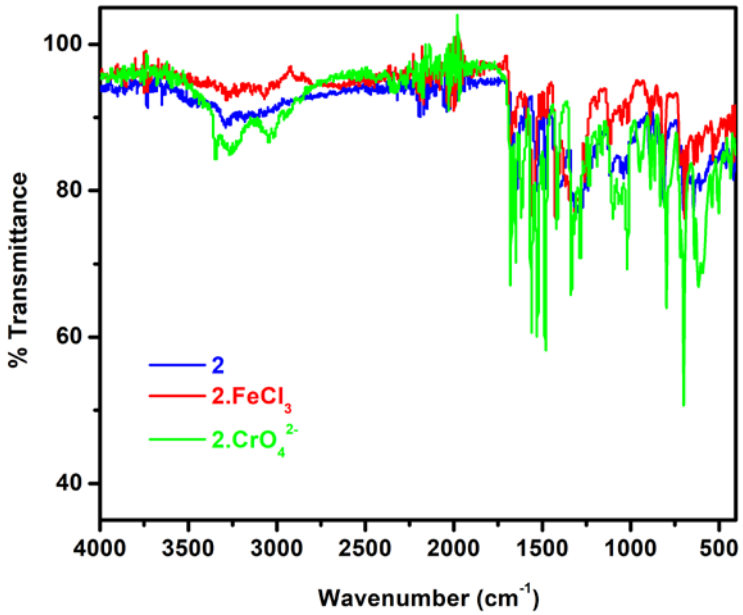

Fig. S22. FT-IR spectra of original sample of **2** (blue trace) and the recovered samples of **2** from the $FeCl_3$ (red trace) and CrO_4^{2-} (green trace) solution.

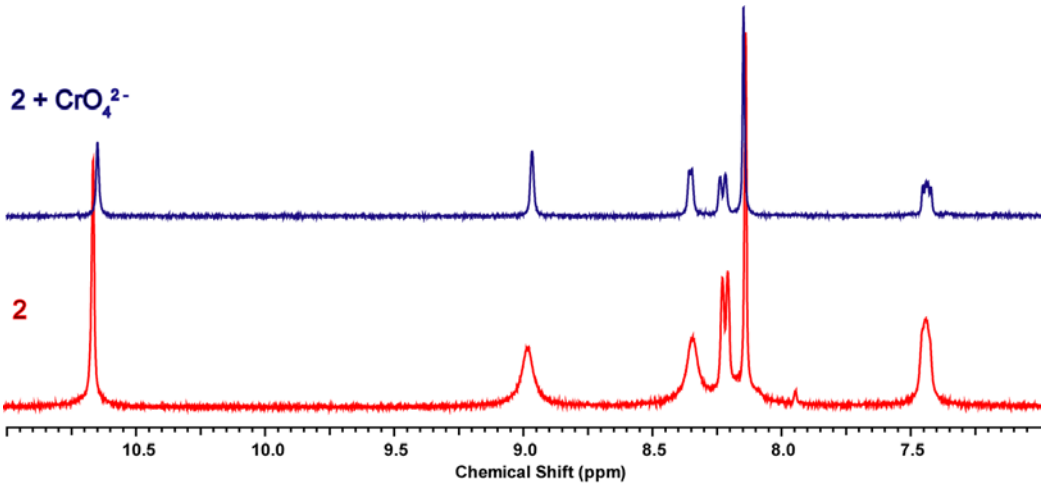

Fig. S23. ^{1}H NMR spectra of coordination polymer **2** before (red trace) and after (purple trace) the addition of 1 equiv of K_2CrO_4 in DMSO-d_6.

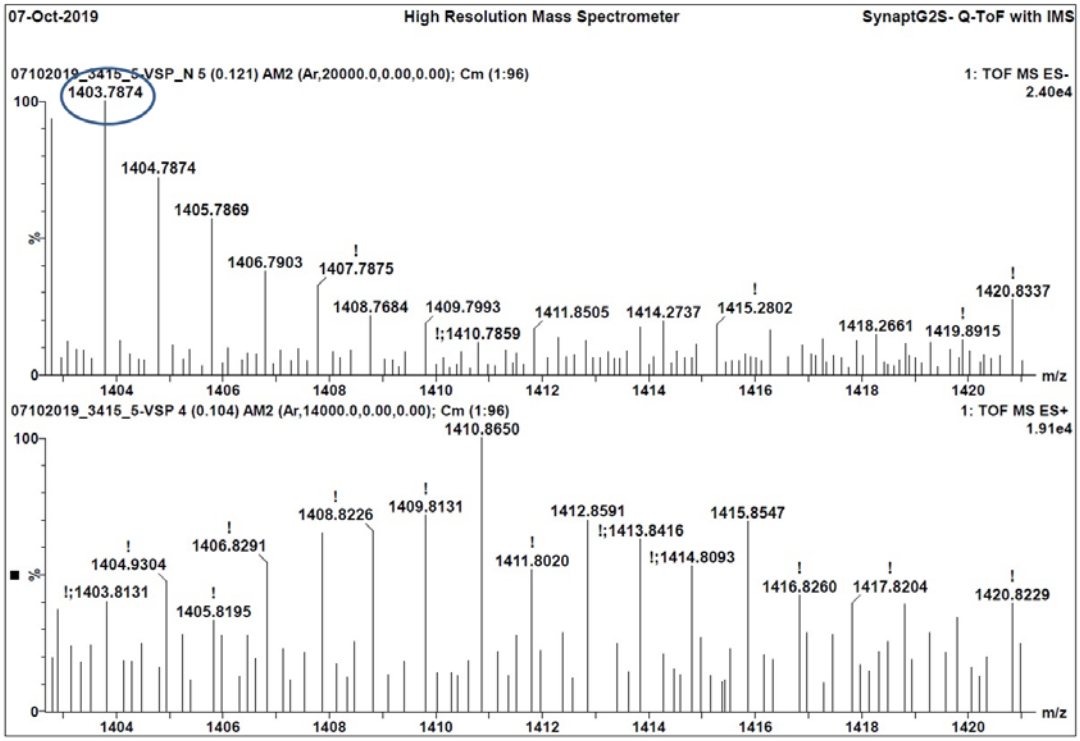

Fig. S24. HR mass spectrum of **1** after the fluorescence quenching with Fe^{3+} ions. MS (ESI-TOF): calculated *m/z* for $[\{M{\cdot}FeCl_3\}–NO_3]^+$ = 1403.0976, found =1403.7874.

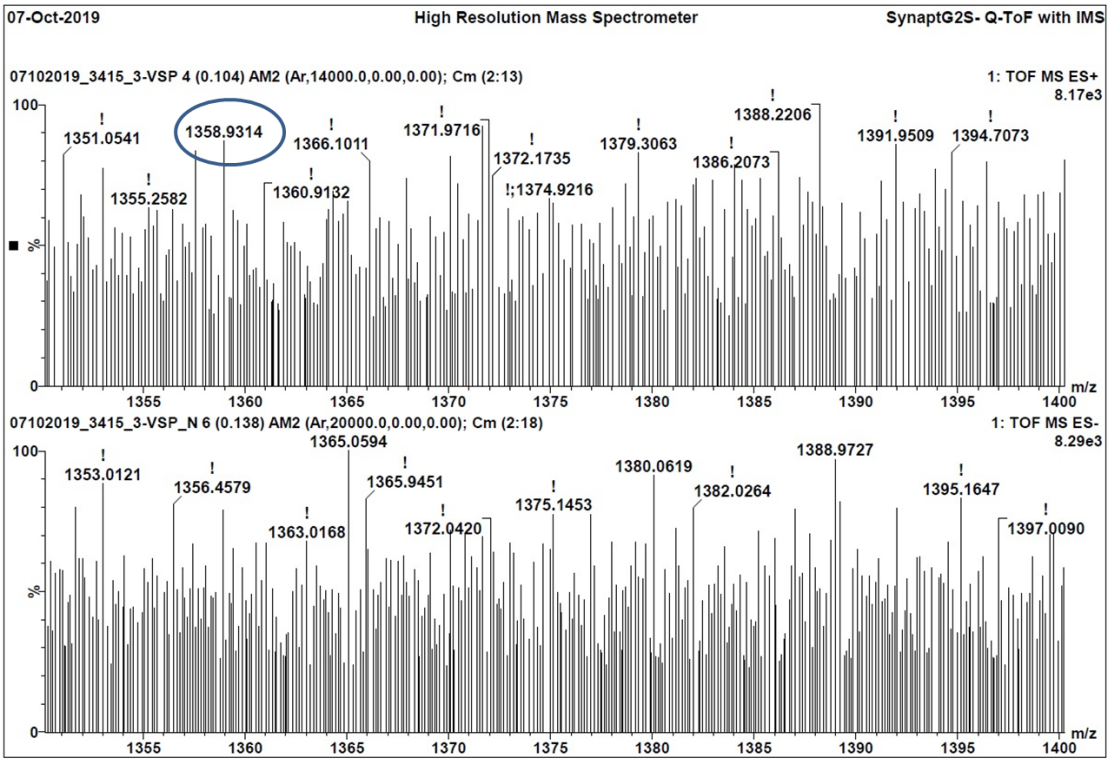

Fig. S25. HR mass spectrum of **1** after the fluorescence quenching with CrO_4^{2-} ions. MS (ESI-TOF): calculated m/z for $[\{M{\cdot}CrO_4^{2-}\}–NO_3]^+$ = 1358.1763, found = 1358.9314.

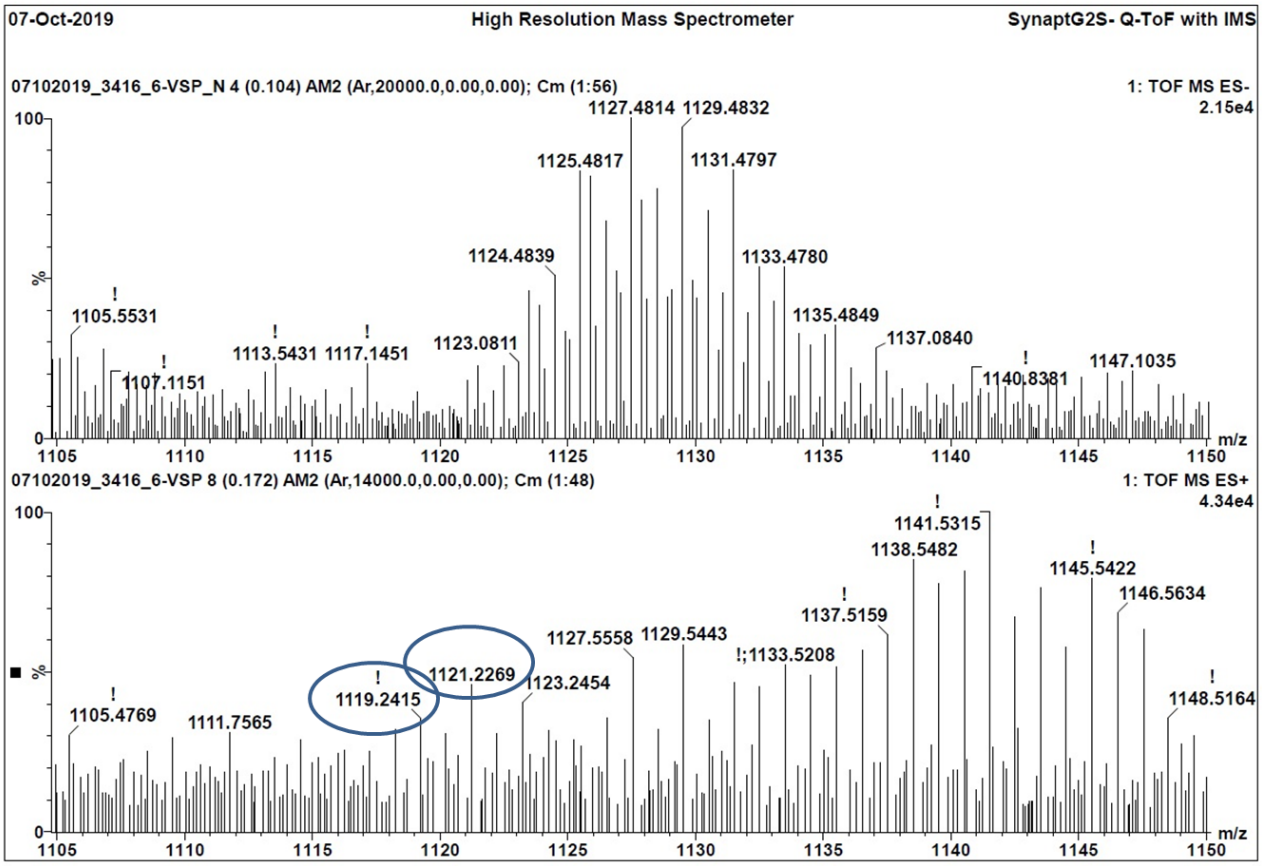

Fig. S26. HR mass spectrum of **2** after the fluorescence quenching with Fe^{3+} ions. MS (ESI-TOF): calculated *m/z* for $[\{M{\cdot}FeCl_3\}–NO_3]^+$ = 1119.0616, found = 1119.2415; $[\{(M+2){\cdot}FeCl_3\}–NO_3]^+$ = 1121.0616, found = 1121.2269.

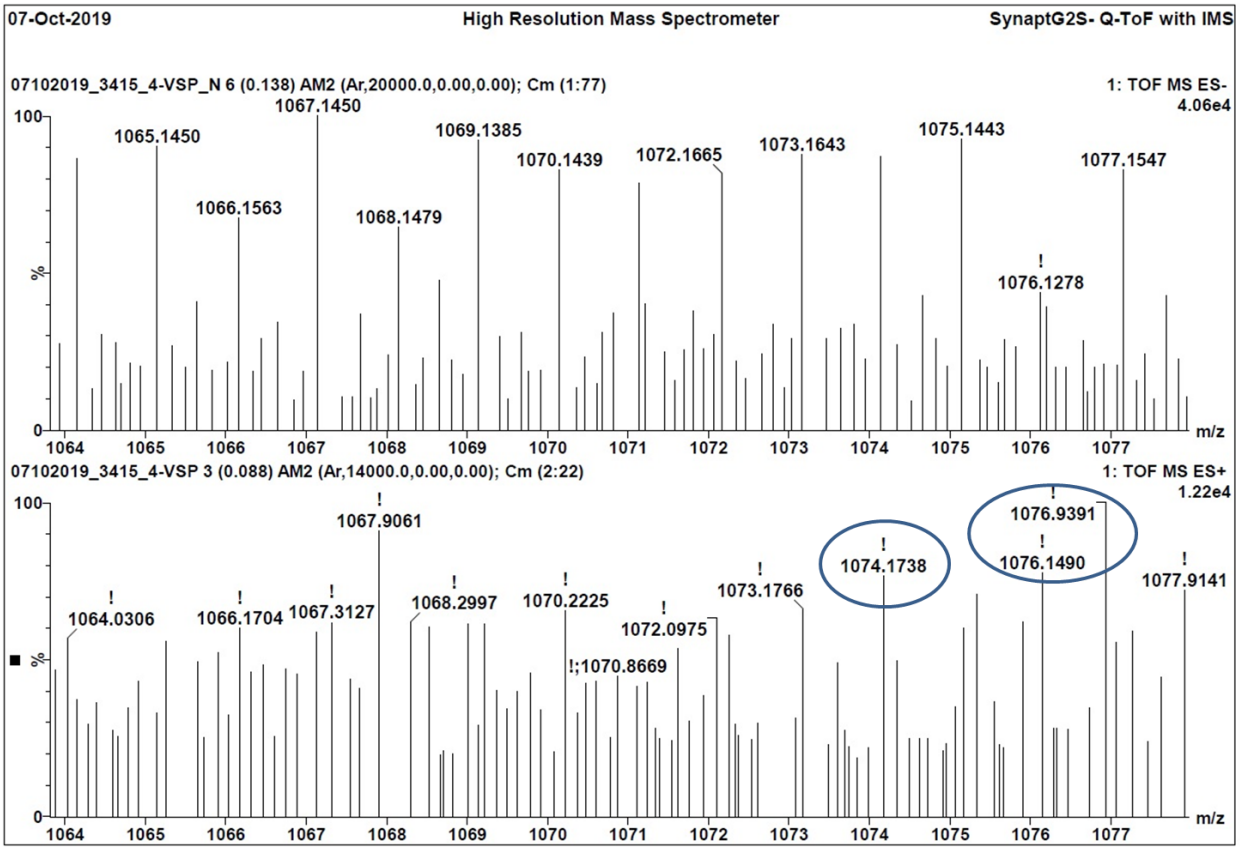

Fig. S27. HR mass spectrum of **2** after the fluorescence quenching with CrO_4^{2-} ions. MS (ESI-TOF): calculated m/z for $[\{M{\cdot}CrO_4^{2-}\}–NO_3]^+$ = 1074.1402, found = 1074.1738; $[\{(M+2){\cdot}CrO_4^{2-}\}–NO_3]^+$ = 1076.1402, found = 1076.1490 and 1076.9391.

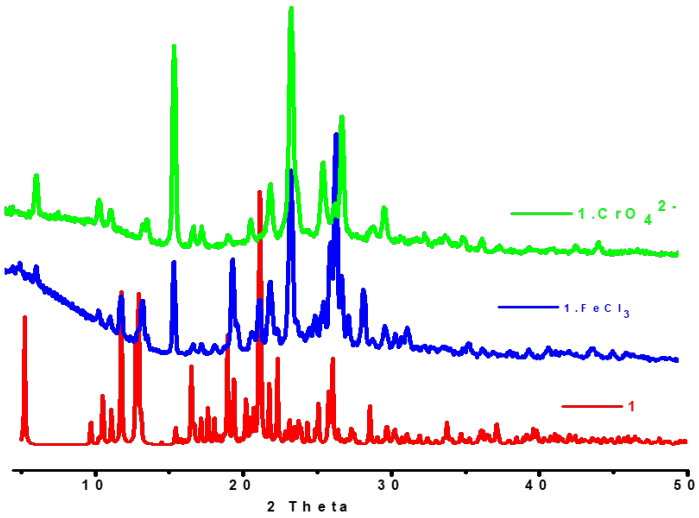

Fig. S28. PXRD patterns of original sample of **1** (red trace) and the recovered samples of **1** from the $FeCl_3$ (blue trace) and CrO_4^{2-} (green trace) solution.

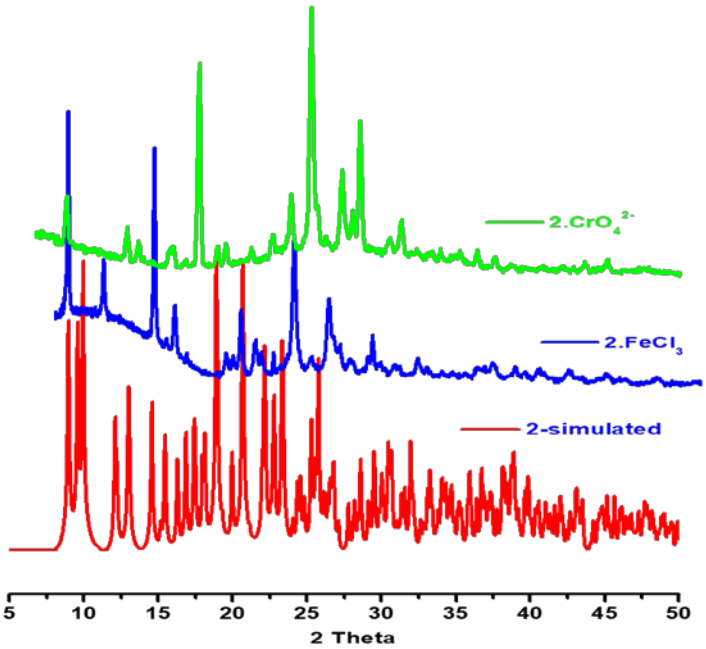

Fig. S29. PXRD patterns of original sample of **2** (red trace) and the recovered samples of **2** from the $FeCl_3$ (blue trace) and CrO_4^{2-} (green trace) solution.

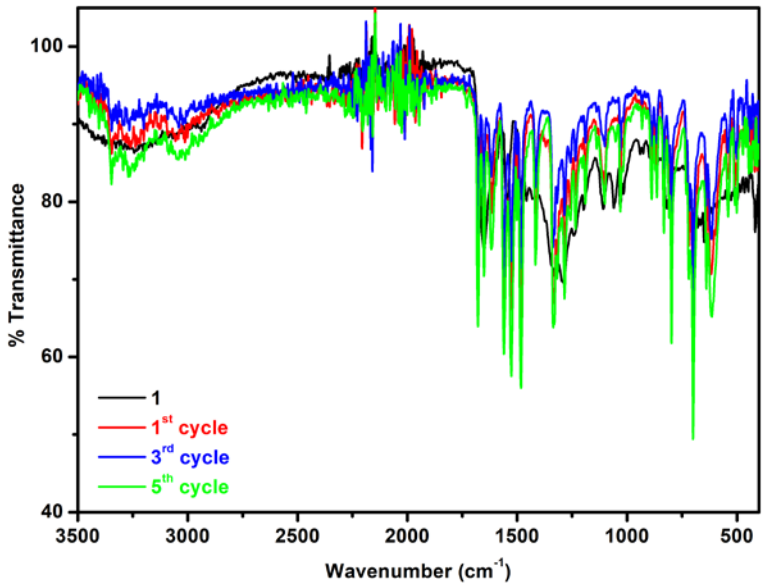

Fig. S30. FT-IR spectra of original sample of **1** and the recovered samples (sensing of CrO_4^{2-} ion) of **1** after recycle experiments.

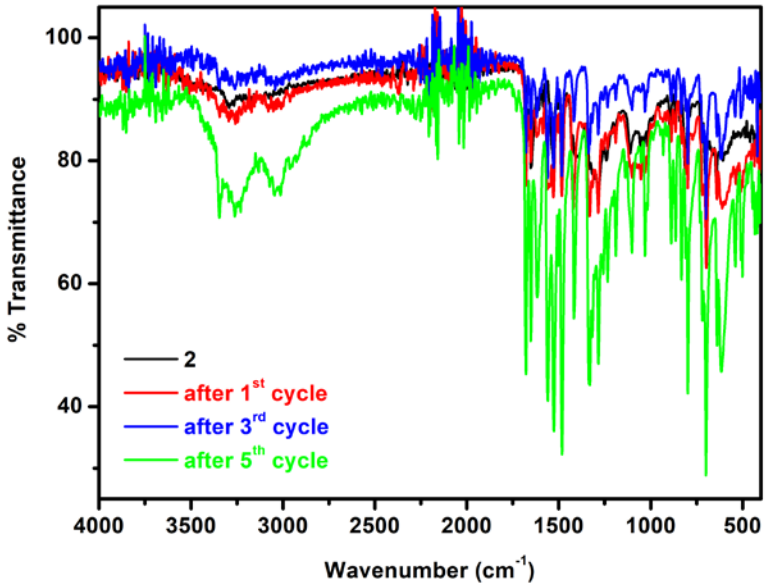

Fig. S31. FT-IR spectra of original sample of **2** and the recovered samples (sensing of CrO_4^{2-} ion) of **2** after recycle experiment.

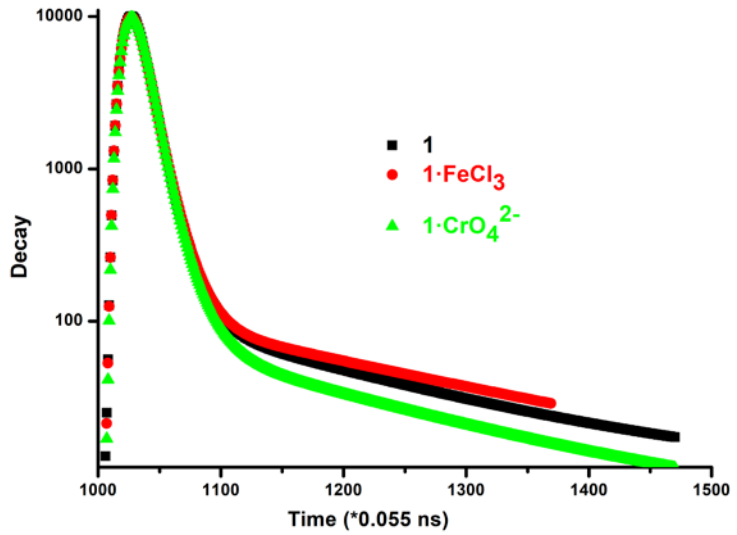

Fig. S32. Decay curves of **1** (black trace) before sensing. The red and green traces represents the decay curves of **1**.$FeCl_3$ and **1**.CrO_4^{2-}, respectively after addition of 60 µM Fe^{3+} or CrO_4^{2-} ion (λ_{ex} = 320 nm; λ_{em} = 450 nm).

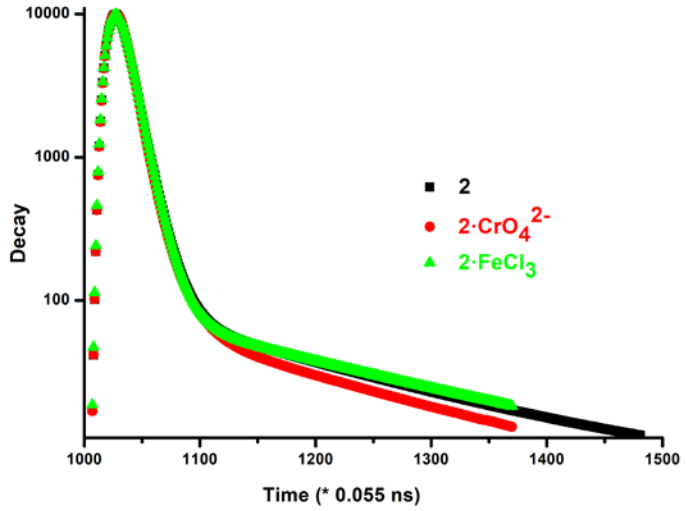

Fig. S33. Decay curves of **2** (black trace) before sensing. The red and green traces represents the decay curves of **2**.$FeCl_3$ and **2**.CrO_4^{2-}, respectively after addition of 60 µM Fe^{3+} or CrO_4^{2-} ion (λ_{ex} = 320 nm; λ_{em} = 450 nm)

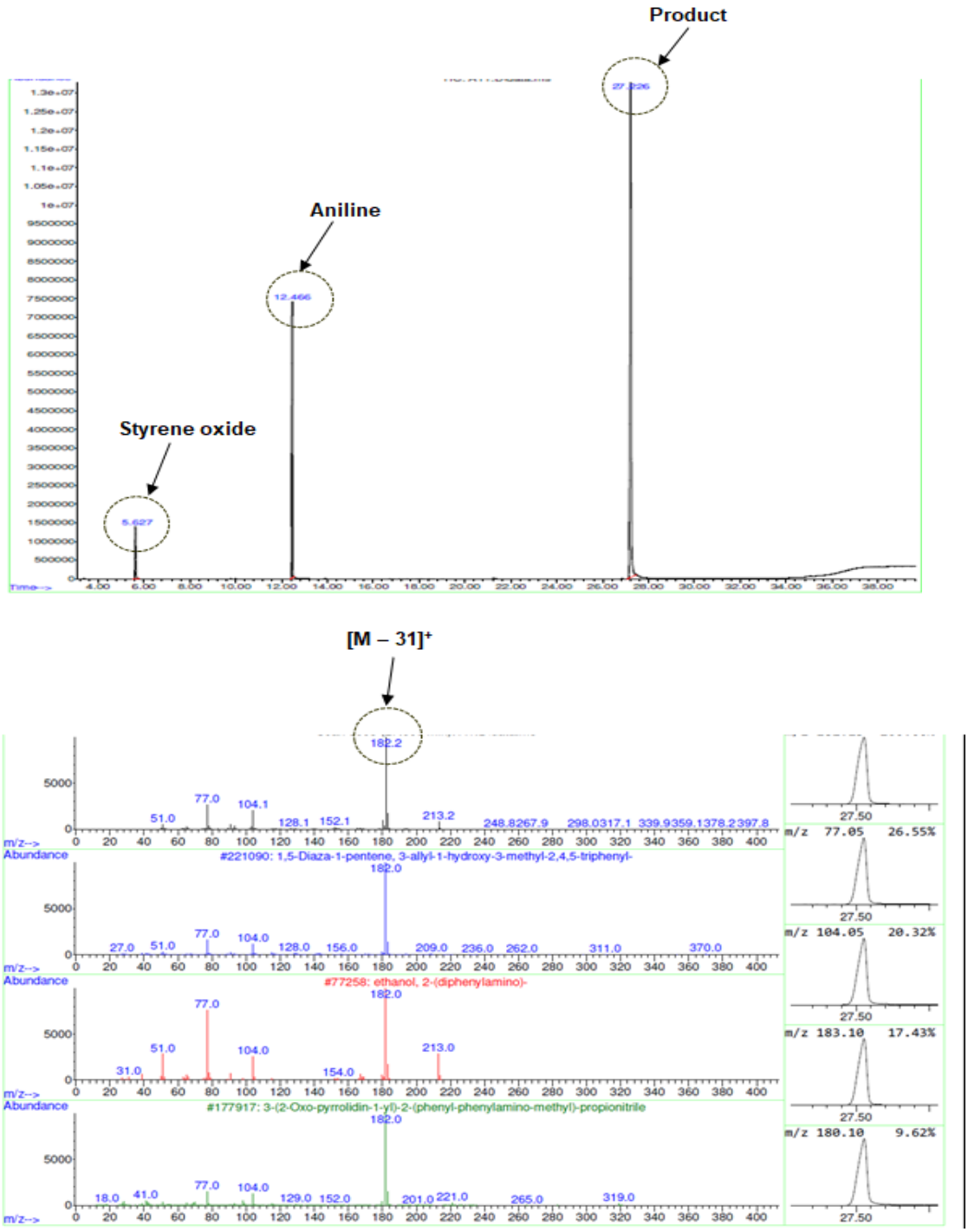

Fig. S34. GC signals of product of styrene oxide ring-opening reaction with aniline using metallacycle **1** as catalyst. The respective MS chromatogram showed regio-isomer having characteristic [M^+ – 31] peak, which confirm the formation of single product (representative one).

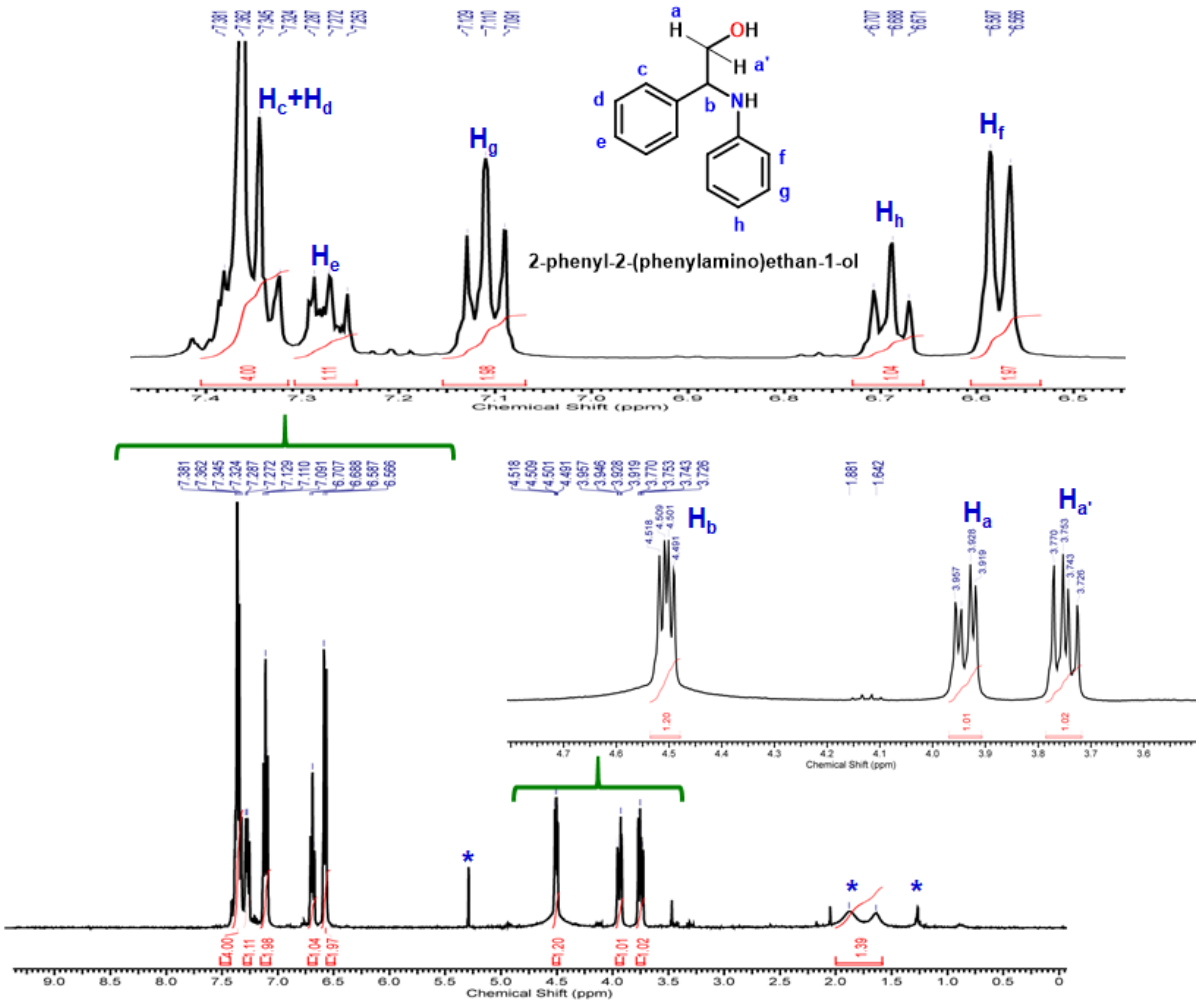

Fig. S35. ^{1}H NMR spectrum of 2-phenyl-2-(phenylamino)ethan-1-ol, a product of styrene oxide ring-opening reaction with aniline using metallacyle **1** as catalyst in $CDCl_3$ (representative one). *Represents the solvent residual peak.

^{1}H NMR (400 MHz, $CDCl_3$) δ = 7.38 –7.32 (m, 4H, H_c+H_d), 7.29 –7.23 (m, 1H, H_e), 7.11 (t, J = 7.6 Hz, 2H, H_g), 6.69 (t, J = 7.6 Hz, 1H, H_h), 6.58 (d, J = 8.4 Hz, 2H, H_f), 4.50 (m, 1H, H_b), 3.93 (dd, J = 6.8, 3.6 Hz, 1H, H_a), 3.73 – 3.77 (dd, J = 6.8, 1H, $H_{a'}$).

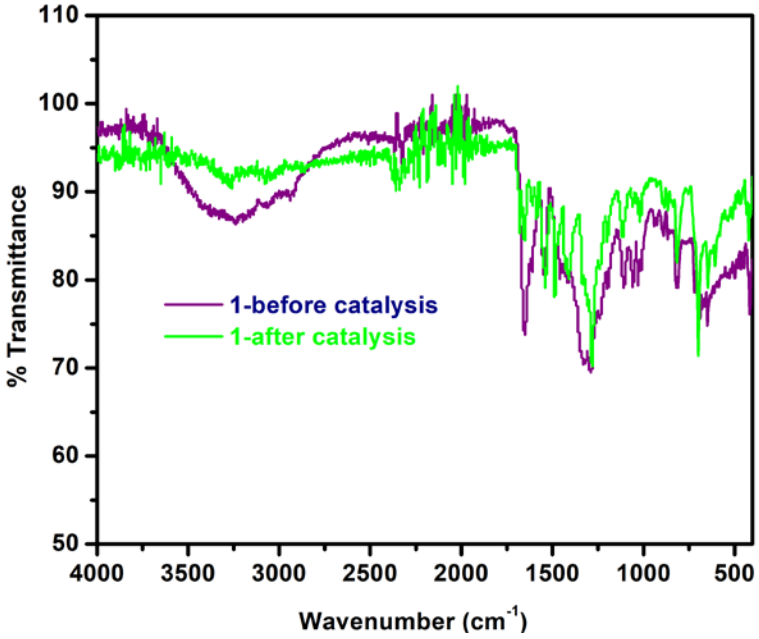

Fig. S36. FTIR spectra of metallacycle **1** before (purple trace) and after the catalysis (green trace) in the ROR of styrene oxide with aniline under solvent free condition.

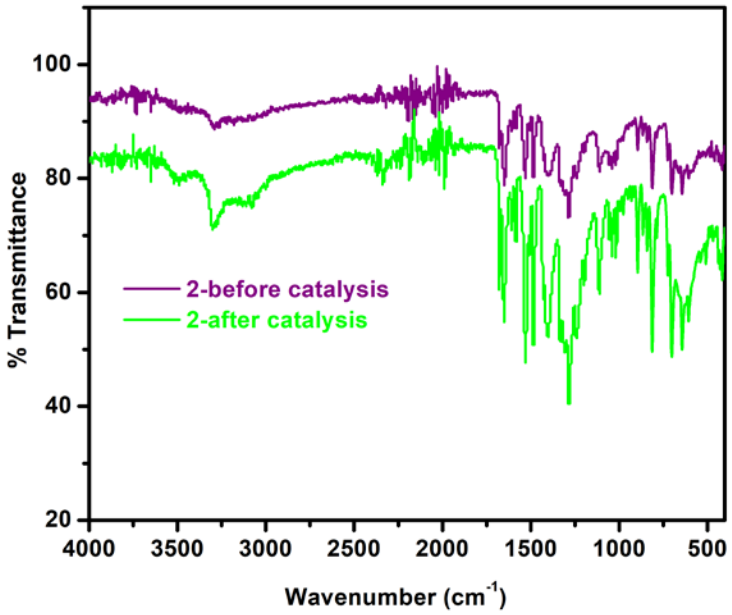

Fig. S37. FTIR spectra of coordination polymer **2** before (purple trace) and after the catalysis (green trace) in the ROR of styrene oxide with aniline under solvent free condition.

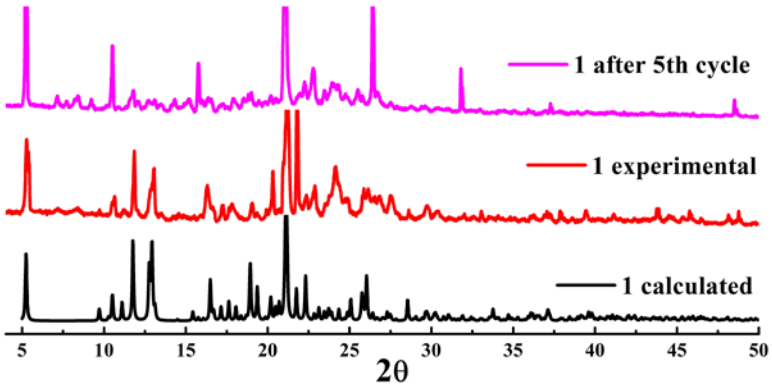

Fig. S38. XRPD pattern for metallacycle **1**, before (red trace) and after RORs of styrene oxide with aniline (violet trace) and their comparison with the simulated pattern obtained from the single crystal structure analysis of **1** (black trace) using Mercury 4.0.

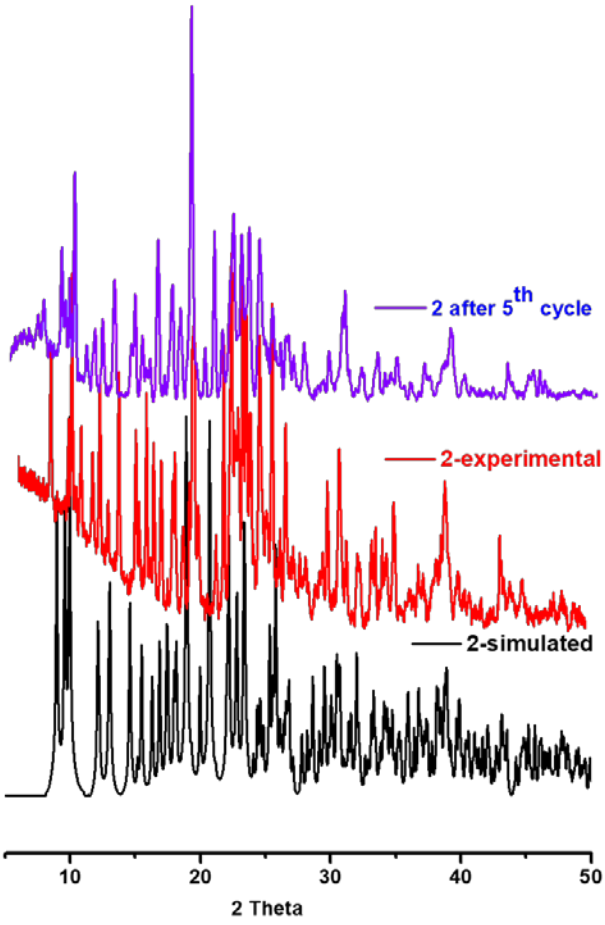

Fig. S39. XRPD pattern for coordination polymer **2**, before (red trace) and after RORs of styrene oxide with aniline (violet trace) and their comparison with the simulated pattern obtained from the single crystal structure analysis of **2** (black trace) using Mercury 4.0.

Table S1. Crystal data and structure refinement for **L**.[1]

Identification code	**L**	**L[1] (reported)**
CCDC No.	1921702	724982
Empirical formula	$C_{18}H_{16}N_4O_3$	$C_{18}H_{14}N_4O_2$
Formula weight	336.35	318.33
Temperature/K	293(2)	100(2)
Crystal system	Triclinic	Triclinic
Space group	$P\bar{1}$	$P\bar{1}$
a/Å	3.9272(3)	5.4387(12)
b/Å	13.5530(8)	6.7043(15)
c/Å	16.0112(9)	10.603(2)
α/°	113.223(5)°	73.402(4)
β/°	95.559(5)°	77.363(4)
γ/°	91.345(5)°	72.933(4)
Volume/Å^3	777.70(9)	350.34(14)
Z	2	1
ρ_{calc}g/cm^3	1.436	1.509
μ/mm^{-1}	0.101	--
F(000)	352	166
Crystal size/mm^3	? × ? × ?	0.25 × 0.22 × 0.15
Radiation (MoKα/ λ)	0.71073	0.103
2Θ range for data collection/°	3.279 to 27.458	100(2)
Index ranges	-5<=h<=4, -16<=k<=16, -19<=l<=20	-6/6, -8/8,-13/8
Reflections collected	7713	1818 /1333/1116
Independent reflections	3023 [R_{int} = 0.0442]	--
Data/restraints/parameters	3023 / 0 / 250	1333/0/113
Goodness-of-fit on F^2	1.074	1.120
Final R indexes [I>=2σ (I)]	R_1 = 0.0728, wR_2 = 0.2147	R_1 = 0.0679, wR_2 = 0.1853
Final R indexes [all data]	R_1 = 0.1102, wR_2 = 0.2420	R_1 = 0.0813, wR_2 = 0.1929
Largest diff. peak/hole / e Å^{-3}	0.354/-0.246	--

[a]$R_1 = \Sigma||Fo| - |Fc||/\Sigma|Fo|$; $wR_2 = \{\Sigma[w(|Fo|^2 - |Fc|^2)_2]/\Sigma[wFo_4]\}^{1/2}$.

Table S2. Selected bond lengths and angles for **1** and **2**.

Bond	Bond lengths (Å)	Bond	Bond Angles (°)
1			
Zn(1)-O(7)	2.0641(17)	N(1)#1-Zn(1)-O(3)	87.28(7)
Zn(1)-N(1)#1	2.076(2)	N(4)-Zn(1)-O(3)	93.96(7)
Zn(1)-N(4)	2.0789(19)	O(7)-Zn(1)-O(5)	89.15(7)
Zn(1)-O(3)	2.1228(17)	N(1)#1-Zn(1)-O(5)	103.83(8)
Zn(1)-O(5)	2.250(2)	N(4)-Zn(1)-O(5)	144.09(8)
Zn(1)-O(4)	2.281(2)	O(3)-Zn(1)-O(5)	86.32(7)
Bond	**Bond Angles (°)**	O(7)-Zn(1)-O(4)	93.57(7)
O(7)-Zn(1)-N(1)#1	86.90(7)	N(1)#1-Zn(1)-O(4)	159.91(8)
O(7)-Zn(1)-N(4)	93.88(7)	N(4)-Zn(1)-O(4)	87.97(7)
N(1)#1-Zn(1)-N(4)	112.06(8)	O(3)-Zn(1)-O(4)	89.81(7)
O(7)-Zn(1)-O(3)	171.56(7)	O(5)-Zn(1)-O(4)	56.12(7)
2			
Bond	**Bond lengths (Å)**	**Bond**	**Bond Angles (°)**
Cd(1)-O(3)	2.335(2)	O(3)#1-Cd(1)-N(4)#1	87.93(9)
Cd(1)-O(3)#1	2.335(2)	N(4)-Cd(1)-N(4)#1	180
Cd(1)-N(4)	2.336(3)	O(3)-Cd(1)-N(1)#2	86.99(9)
Cd(1)-N(4)#1	2.336(3)	O(3)#1-Cd(1)-N(1)#2	93.01(9)
Cd(1)-N(1)#2	2.353(3)	N(4)-Cd(1)-N(1)#2	88.45(9)
Cd(1)-N(1)#3	2.353(3)	N(4)#1-Cd(1)-N(1)#2	91.55(9)
Bond	**Bond Angles (°)**	O(3)-Cd(1)-N(1)#3	93.01(9)
O(3)-Cd(1)-O(3)#1	180	O(3)#1-Cd(1)-N(1)#3	86.99(9)
O(3)-Cd(1)-N(4)	87.93(9)	N(4)-Cd(1)-N(1)#3	91.55(9)
O(3)#1-Cd(1)-N(4)	92.07(9)	N(4)#1-Cd(1)-N(1)#3	88.45(9)
O(3)-Cd(1)-N(4)#1	92.07(9)	N(1)#2-Cd(1)-N(1)#3	180.00(12)

Symmetry transformations used to generate equivalent atoms: For **1**: #1 1-x,2-y,1-z. For **2**: #1 -x+2,-y+1,-z #2 x+1,y,z-1 #3 -x+1,-y+1,-z+1 #4 x-1,y,z+1.

Table S3. Hydrogen bonds and short contacts for **1** and **2**.

D–H...A	d(D-H)/Å	d(H-A)/Å	d(D-A)/Å	<D-H-A/°
		1		
N3–H3...O9$^{\#1}$	0.86	2.10	2.936(3)	165
N2–H2...O8	0.86	2.12	2.923(3)	156
N2–H2...O10	0.86	2.51	3.251(3)	144
N2–H2...N8	0.86	2.67	3.509(3)	165
C5–H5...O7$^{\#1}$	0.93	2.58	3.035(3)	111
C17–H17...O3	0.93	2.46	3.069(3)	123
C18–H18...O7	0.93	2.52	3.096(3)	121
C1–H1...O6$^{\#2}$	0.93	2.63	3.252(3)	125
C3–H3A...O1	0.93	2.26	2.840(3)	120
C16–H16...O6$^{\#3}$	0.93	2.61	3.525(3)	168
C15–H15...O2	0.93	2.33	2.810(3)	112
C19–H19C...O6$^{\#4}$	0.96	2.65	3.596(4)	169
C20–H20A...O2$^{\#3}$	0.96	2.65	3.209(4)	118
C23–H23B...O10$^{\#5}$	0.96	2.59	3.422(5)	145
		2		
C(3)-H(3)...O(1)	0.93	2.26	2.820(4)	118
C(15)-H(15)...O(2)	0.93	2.33	2.828(4)	113
C(17)-H(17)...O(3)	0.93	2.59	3.197(4)	123
C(18)-H(18)...O(6)	0.93	2.58	3.307(4)	136
N(2)-H(2A)...O(5)$^{\#3}$	0.84(3)	2.69(3)	3.498(5)	161(3)
N(2)-H(2A)...O(6)$^{\#3}$	0.84(3)	2.36(3)	3.109(4)	148(3)
N(3)-H(3A)...N(6)	0.86(3)	2.71(3)	3.559(5)	166(3)
N(3)-H(3A)...O(4)	0.86(3)	2.46(3)	3.220(4)	147(3)
N(3)-H(3A)...O(6)	0.86(3)	2.23(3)	3.026(4)	152(3)

Symmetry transformations used to generate equivalent atoms: For **1**. #1 1-x,2-y,1-z; #2 -1+x,+y,1+z; #3 1-x,1-y,-z; #4 2-x,2-y,-z; #5 2-x,2-y,1-z. For **2**: #1 -x+2,-y+1,-z #2 x+1,y,z-1 #3 -x+1,-y+1,-z+1 #4 x-1,y,z+1

Table S4. Comparison of various fluorescent CPs / MOFs / metallacycles for sensing of Fe^{3+} and CrO_4^{2-} and other relevant ions.

CPs / MOFs / metallacycles	Analyte	Quenching Constant (K_{sv}, M^{-1})	Limit of detection (μM)	Solvent	Ref.
$[Zn_2\{(\mathbf{L})_2(DMF)_2(NO_3)_2\}]\cdot(NO_3)_2$ (**1**) $[\{Cd_1(\mathbf{L})_2(DMF)_2\}.(NO_3)_2]_n$ (**2**)	Fe^{3+}/ CrO_4^{2-}	2.34×10^6/ 6.72×10^5 3.25×10^6/ 6.94×10^5	0.153 / 0.205 0.193 / 0.155	water	In this work
$[Cd_6(\mathbf{L^1})_4(1,3\text{-bit})_2(H_2O)_4]_n$ (**3a**) $[Cd(HL^1)(4,4'\text{-bbibp})]_n$ (**3b**) $[Cd_3(\mathbf{L^1})_2(1,4\text{-bimb})_2(H_2O)_2]_n$ (**3c**) $[Cd(HL^1)(4,4\text{-bidpe})]_n$ (**3d**) $[Cd_3(\mathbf{L^1})_2(1,1\text{-bbi})(H_2O)_4]_n$ (**3e**)	Fe^{3+}/CrO_4^{2-}	3.64×10^4/ 2.23×10^4 3.42×10^4/ 9.54×10^4 2.07×10^4/ 2.23×10^4 3.83×10^4/ 3.76×10^4 2.36×10^4/ 1.87×10^4	0.82 / 1.35 0.88 / 0.31 1.45 / 1.34 0.78 / 0.98 1.27 / 1.61	water	S15
$[Ln(H\mathbf{L^2})_{1.5}(H_2O)(DMF)]\cdot 2H_2O$ (Ln = Gd^{3+} (**4a**), Sm^{3+} (**4b**), Dy^{3+} (**4c**), Eu^{3+} (**4d**) and Tb^{3+} (**4e**)	Fe^{3+}	1×10^4 (for **4d**) 9.92×10^3 (for **4e**)	1.03 (for **4d**) 1.04 (for **4e**)	water	S16
$[\{Zn_2(\mathbf{L^3})_{1.5}Cl_5\}\cdot 0.5Cl\cdot H_2O]$ (**5**)	Fe^{3+} / IO_4^-	0.23×10^5 & 1.5×10^6 / 1.4×10^3	2.6 / 63	DMF	S14
$[H_2N(CH_3)_2]_2[Zn_2\mathbf{L^4}(HPO_3)_2]$ (**6**)	Fe^{3+}/ $Cr_2O_7^{2-}$	3.96×10^5 / 4.44×10^4	1.16×10^{-4}/ 1.09×10^{-3} (in molar unit)	water	S17
$\{[Zn(\mathbf{L^5})(H_2O)_2]\cdot H_2O\}_n$ (**7a**) $[Cd(\mathbf{L^5})(H_2O)_2]\cdot 4H_2O\}_n$ (**7b**)	Fe^{3+}/ CrO_4^{2-}/ $Cr_2O_7^{2-}$/TNP	1.09×10^5/4.1×10^4/ 9.1×10^4/9.77×10^4 7.2×10^4/3.03×10^4/ 3.58×10^4/8.52×10^4	0.56 / 5.7/ 7.3/0.63 0.78/6.8/ 8.2/0.75	water	S18
$[Cd\mathbf{L^6}(H_2O)]\cdot{}_2H_2O$ (**8a**) $[Cd\mathbf{L^6}(H_2O(4,4'\text{-bipy})_{0.5}]\cdot H_2O$ (**8b**) $[Cd\mathbf{L^6}(H_2O)_2]\cdot{}_{0.5}H_2bdc]$ (**8c**)	Fe^{3+}	3.529×10^4 3.619×10^4 3.260×10^4	4.32 3.28 1.23	Water	S19
$[H_2bpy]_{0.5}(Cd_3(OH)(\mathbf{L^7})_2(bpy)(H_2O)_2]\cdot(bpy)_{0.5}\cdot 2H_2O$ (**9**)	Fe^{3+} /TNP	5.27×10^4 /2.34×10^4	1.34 / 0.21	Ethanol	S20
$\{Zn_2(NO_3)_2(4,4'\text{-bpy})_2(TBA)\}$ (**10**)	Fe^{3+} /PA	7.48×10^3 / 4.28×10^4	7.18 /6.02	Water	S21
$\{[Zn(\mathbf{L^8})_{0.5}(bimb)]\cdot 2H_2O\cdot 0.5(CH_3)_2NH\}_n$ (**11a**) $\{[Zn(\mathbf{L^8})_{0.5}(bimmb)]\cdot 2H_2O\}_n$ (**11b**) $\{[Zn(\mathbf{L^8})_{0.5}(btdpe)]\cdot H_2O\}_n$ (**11c**) $[Zn(\mathbf{L^8})_{0.5}(bidpe)]_n$ (**11d**)	Fe^{3+}/ CrO_4^{2-}/ $Cr_2O_7^{2-}$	6.28×10^4 /5.04×10^4 /5.68×10^4 4.07×10^4 /6.76×10^4 /7.35×10^4 5.1×10^4 /6.47×10^4 /5.55×10^4 4.97×10^4 /5.54×10^4 /6.20×10^4	0.48 /0.60 /0.53 0.74 /0.44 /0.41 0.59 /0.46/ 0.54 0.64 /0.54/ 0.48	water	S22
$\{[Zn_3(mtrb)_3(btc)_2]\cdot 3H_2O\}_n$ (**12**)	Fe^{3+}/ CrO_4^{2-}/ $Cr_2O_7^{2-}$/	6.50×10^3 /2.77×10^3 / 4.62×10^3 /$3.26 \times$	1.78/ 2.83 / 4.52 / 0.22	MeOH	S23

	TNP/ANP	10^4 / 7.92×10^3	/4.12		
$\{[Zn_3(\mathbf{L^9})(OH)(H_2O)_5]\cdot NMP\cdot 2H_2O\}_n$ (**13a**) $\{[H_2N(Me)_2][Zn_2(\mathbf{L^9})(H_2O)]\cdot DMF\cdot H_2O\}_n$ (**13b**) $\{[Co_5(\mathbf{L^9})_2(H_2O)_{11}]\cdot 2H_2O\}_n$ (**13c**) $\{[Mn_5(\mathbf{L^9})_2(H_2O)_{12}]\cdot 6H_2O\}_n$ (**13d**)	Fe^{3+}/ CrO_4^{2-}/ $Cr_2O_7^{2-}$/ MnO_4^{2-}	With **13a** 4.7×10^4/1.3×10^4 6.6×10^4 /1.1×10^4	7.7×10^{-5}/ 4.29×10^{-4}/ 6.05×10^{-5}/ 3.38×10^{-4} (in molar unit)	Water	S24

Abbreviation: **L** = N,N'-bis-(3-pyridyl)terephthalamide, $H_3\mathbf{L^1}$ = 5-(2-carboxylphenoxy)isophthalic acid, 1,3-bit = 1,3-bis(l-imidazoly)toluene, 4,4'-bbibp = 4,4'-bis(benzoimidazo-1-ly)biphenyl, 1,4-bimb = 1,4-bis(imidazol-l-ylmethyl)benzene, 4,4'-bidpe = 4,4'-bis(imidazolyl)diphenyl ether, 1,1'-bbi = 1,1'-(1,4-butanediyl)bis(imidazole), $H_3\mathbf{L^2}$ = 5-(3',5'-dicarboxylphenyl) nicotinic acid), $\mathbf{L^3}$ = 1,3-bis(2,6-diisopropyl-4-(pyridin-4-yl)phenyl)-1Himidazol-3-ium chloride/bromide, where $H_2\mathbf{L^4}$= 2,3,5,6-tetramethyl-[1,1:4,1"-terphenyl]-4,4"-dicarboxylic acid, 4,4'-bipy = 4,4'-bipyridine, H_2bdc = 1,4-benzene dicarboxylic acid, $H_2\mathbf{L^5}$ = 5-(4-pyridylamino)isophthalic acid, $H_2\mathbf{L^6}$ = 5-(4-pyridyl)-methoxylisophthalic acid, $H_3\mathbf{L^7}$ = 3-(3,5-dicarboxylphenyl)-4-carboxylpyridine, H_2TBA = 4-(1Htetrazol-5-yl)-benzoic acid, $H_4\mathbf{L^8}$ = 5,5'-(1,4-xylylenediamino)diisophthalic acid, bimb = 1,4-bis(imidazol-1-yl)-butane, bimmb = 1,4-bis(imidazol-1-ylmethyl)benzene, btdpe = 4,4'-bis(4H-1,2,4-triazol-4-yl)diphenyl ether, bidpe = 4,4'-Bis(imidazolyl)diphenyl ether), mtrb = 1,3-bis(1,2,4-triazole-4-ylmethyl)benzene, btc = 1,3,5-benzenetricarboxylate), ANP = 2-amino-4-nitrophenol, TNP = 2,4,6-trinitrophenol, $H_5\mathbf{L^9}$ (H_5L = 2,4-di(3',5'-dicarboxylphenyl)benzoic acid).

Table S5. The detailed ICP studies of metallacycle **1** and coordination polymer **2** after sensing of Fe^{3+} and CrO_4^{2-} ions.

Sample	Fe^{3+} (%)	Cr^{6+} (%)
1·$FeCl_3$	1.3	--
2·$FeCl_3$	2.5	--
1·CrO_4^{2-}	--	1.1
2·CrO_4^{2-}	--	1.9

Table S6. Fluorescence lifetime measurements data for the coordination compounds **1** and **2**, before and after sensing of Fe^{3+} and CrO_4^{2-} ions.

Sr. No.	Complex	B_1	τ_1(ns)	B_2	τ_2(ns)	B_3	τ_3 (ns)	τ_{avg} (ns)	χ^2
1.	**1**	0.153	0.368	0.028	0.845	0.00055	11.65	0.4765	1.147
2.	**1 + Fe^{+3}**	0.129	0.312	0.06	0.68	0.0006	12.92	0.4752	1.009
3.	**1 + CrO_4^{2-}**	0.16	0.396	0.02	0.898	0.0004	9.76	0.4729	1.005
4.	**2**	0.125	0.292	0.07	0.644	0.0005	9.51	0.4396	1.055
5.	**2 + Fe^{+3}**	0.136	0.367	0.04	0.702	0.0004	10.94	0.4759	1.003
6.	**2 + CrO_4^{2-}**	0.148	0.314	0.049	0.675	0.0005	8.03	0.4228	1.113

Table S7. The dimensions of the metallacycle and guest analytes employed in this investigations were calculated by the selections of two appropriate atoms and their centre-to-centre distance was measured by Chem3D[6] followed by the addition of their van der Walls radii.[7–11]

S.No.	Substrates	Molecular dimensions
*1.	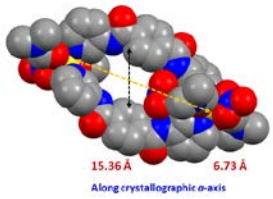	6.73 × 15.36 $Å^2$
*2.	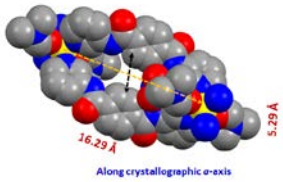	5.29 × 16.29 $Å^2$
3.	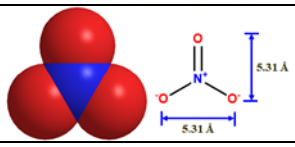	5.31 × 5.31 $Å^2$
4.	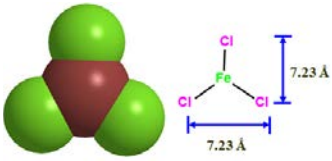	7.23 × 7.23 $Å^2$

5.	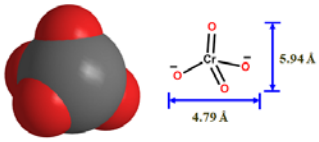	5.94 × 4.79 Å^2

*Cavity size for Zn(II) metallacycle **(1)** and Cd(II) coordination polymer **(2)** were estimated by X-ray diffraction analysis.[12–14]

Table S8. Control experiments for the ROR of styrene oxide with aniline using different salts of zinc and cadmium metal atom.

Entry	Epoxide	Amine	Product	Metal salt	Yield [%]
1.	S.O.	Aniline	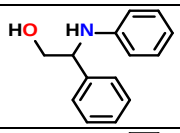	$Zn(NO_3)_2.6H_2O$	23
2.	S.O.	Aniline	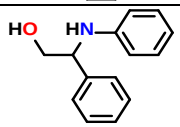	$ZnCl_2$	27
3.	S.O.	Aniline	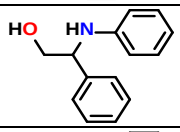	$Zn(OAc)_2.6H_2O$	26
4.	S.O.	Aniline	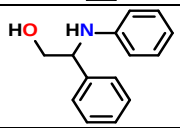	$Cd(NO_3)_2.4H_2O$	20
5.	S.O.	Aniline	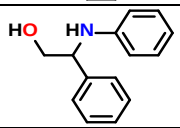	$CdCl_2$	20
6.	S.O.	Aniline	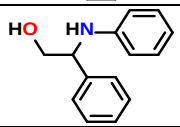	$Cd(OAc)_2$	23
7.	S.O.	Aniline	No reaction	Without catalyst	No conversion

[a]Products were quantified by using gas chromatograph. C.O. and S.O. are stand for the cyclohexane oxide and styrene oxide, respectively.

References.

1. N.N. Adarsh, D.K. Kumar, E. Suresh, P. Dastidar, *Inorganica Chim. Acta*, 2010, **363,** 1367–1376.

2. N.N. Adarsh, P. Dastidar, *Cryst. Growth Des.*, 2011, **11**, 328–336.

3. A. Ganguly, B.K. Paul, S. Ghosh, S. Kar, N. Guchhait, *Analyst,* 2013, **138**, 6532–6541.

4. H. A. Benesi, J. H. Hildebrand, *J. Am. Chem. Soc*. 1949, **71**, 2703–2707.

5. C. Liang, W. Bu, C. Li, G. Men, M. Deng, Y. Jiangyao, H. Sun, S. Jiang, *Dalton Trans.* 2015, **44**, 11352–11359.

6. Chem3D Ultra 15.1, Cambridge Soft Corporation, Cambridge, MA, 2015.

7. G. Kumar, R. Gupta, *Inorg. Chem.*, 2013, **52**, 10773−10787.

8. G. Kumar, R. Gupta, *Inorg. Chem.,* 2012, **51**, 5497−5499.

9. J.-M. Gu, T.-H. Kwon, J.-H. Park, S. Huh, *Dalton Trans.,* 2010, **39**, 5608–5610.

10. J.-M. Gu, W.-S. Kim, S. Huh, *Dalton Trans.*, 2011, **40**, 10826–10829.

11. X.-M. Lin, T.-T. Li, L.-F. Chen, L. Zhang, C.-Y. Su, *Dalton Trans.*, 2012, **41**, 10422–10429.

12. M. Ogawa, M. Nagashima, H. Sogawa, S. Kuwata, T. Takata, *Org. Lett.*, 2015, **17**, 1664−1667.

13. M.J. Langton, C.J. Serpell, P.D. Beer, *Angew. Chem. Int. Ed.*, 2016, **55**, 1974–1987.

14 G. Kumar, R. Guda, A. Husain, R. Bodapati, S.K. Das, *Inorg. Chem.,* 2017, **56**, 5017–5025.

15. C. Fan, Z. Zong, X. Meng, X. Zhang, X. Zhang, D. Zhang, C. Xu, H. Wang and Y. Fan, *CrystEngComm*, 2019, **21**, 4880**–**4897.

16. F. Zhao, X.-Y. Guo, Z.-P. Dong, Z.-L. Liu and Y.-Q. Wang, *Dalton Trans*., 2018, **47**, 8972–8982.

17. S.-F. Tang and X. Hou, *Cryst. Growth Des*. 2019, **19**, 45−48.

18. A.-M. Zhou, H. Wei, W. Gao, J.-P. Liu and X.-M. Zhang, *CrystEngComm,* 2019, ***21***, 5185-5194.

19. X. Guo, J. Xu, J. Sun, X. Chen, L. Wang and Y. Fan, *CrystEngComm*, 2019, **21**, 1001–1008.

20. W. Gao, F. Liu, C.-W. Pan, X.-M. Zhang, J.-P. Liu and Q.-Y. Gao, *CrystEngComm*, 2019, **21**, 1159–1167.

21. X. Zhang, X. Zhuang, N. Zhang, C. Ge, X. Luo, J. Li, J. Wu, Q. Yang and R. Liu, *CrystEngComm*, 2019, **21**, 1948–1955.

22. C. Xu, C. Bi, Z. Zhu, R. Luo, X. Zhang, D. Zhang, C. Fan, L. Cui and Y. Fan, *CrystEngComm*, 2019, **21**, 2333–2344.

23. Y.-Q. Zhang, V. A. Blatov, T.-R. Zheng, C.-H. Yang, L.-L. Qian, K. Li, B.-L. Li and B. Wu, *Dalton Trans*., 2018, 47, 6189–6198.

24. Y.-T. Yan, W.-Y. Zhang, F. Zhang, F. Cao, R.-F. Yang, Y.-Y. Wang and L. Hou, *Dalton Trans*., 2018, **47**, 1682–1692.

****